CANCER

The tumor microenvironment and Immunoscore are critical determinants of dissemination to distant metastasis

Bernhard Mlecnik,[1,2,3]* Gabriela Bindea,[1,2,3]* Amos Kirilovsky,[1,2,3]* Helen K. Angell,[1,2,3,4] Anna C. Obenauf,[5] Marie Tosolini,[1,2,3] Sarah E. Church,[1,2,3] Pauline Maby,[1,2,3] Angela Vasaturo,[1,2,3] Mihaela Angelova,[1,2,3] Tessa Fredriksen,[1,2,3] Stéphanie Mauger,[1,2,3] Maximilian Waldner,[6] Anne Berger,[7] Michael R. Speicher,[5] Franck Pagès,[1,2,3,8] Viia Valge-Archer,[9] Jérôme Galon[1,2,3]†

Although distant metastases account for most of the deaths in cancer patients, fundamental questions regarding mechanisms that promote or inhibit metastasis remain unanswered. We show the impact of mutations, genomic instability, lymphatic and blood vascularization, and the immune contexture of the tumor microenvironment on synchronous metastases in large cohorts of colorectal cancer patients. We observed large genetic heterogeneity among primary tumors, but no major differences in chromosomal instability or key cancer-associated mutations. Similar patterns of cancer-related gene expression levels were observed between patients. No cancer-associated genes or pathways were associated with M stage. Instead, mutations of *FBXW7* were associated with the absence of metastasis and correlated with increased expression of T cell proliferation and antigen presentation functions. Analyzing the tumor microenvironment, we observed two hallmarks of the metastatic process: decreased presence of lymphatic vessels and reduced immune cytotoxicity. These events could be the initiating factors driving both synchronous and metachronous metastases. Our data demonstrate the protective impact of the Immunoscore, a cytotoxic immune signature, and increased marginal lymphatic vessels, against the generation of distant metastases, regardless of genomic instability.

INTRODUCTION

Metastasis is a major clinical issue in colorectal cancer (CRC), because more than 90% of patients with synchronous metastases die within 5 years (*1*). An improved understanding of the processes leading to tumor metastatic invasion and development is required to develop novel treatment paradigms for patients with late-stage tumors. However, the extensive interactions between tumor cells, their microenvironment, and surrounding tissues during their dissemination have complicated efforts to dissect the metastatic process (*2*, *3*). Metastatic tumor cells must successfully negotiate a series of complex steps, leading to their establishment in a foreign tissue environment. Many important genes and pathways implicated in malignant progression and migration have been described (*4*). Genetic instability, gene expression changes, and the resulting heterogeneity within the tumor cell populations have all been associated with the process of invasion and metastasis (*5*). Whereas some current models consider metastasis to arise from cell-autonomous alterations in the cancer cell genome, alternative views propose that metastatic traits are acquired through the exposure of cancer cells to paracrine signals received within the tumor microenvironment (*2*–*4*). The vast diversity of intratumoral immune cell populations (*6*–*14*) and the often transient and elusive nature of paracrine signals have hindered the elucidation of the role of the tumor microenvironment on the metastatic potential of cancer cells (*10*, *13*). Murine studies have shown that the immune system maintains circulating tumor cells in a state of dormancy, preventing distant metastases (*15*–*17*), and may also promote in situ dormancy of tissue micrometastases (*18*). Evidence of this mechanism is supported in humans by our previous data showing a major role of cytotoxic and memory T cells in predicting survival of cancer patients (*6*, *19*), including early-stage cancer patients (*20*). Here, we analyzed mutations, genomic instability, malignant cell–related gene expression, lymphatic vessel density (LVD), blood vessel density (BVD), and the complex immune contexture of the tumor microenvironment (*6*–*10*, *16*, *21*) on large cohorts of CRC patients (table S1). Our aim was to perform a comprehensive analysis of both primary tumors and microenvironment factors in relation to the presence of synchronous distant metastases.

RESULTS

Similar patterns of genomic alterations are found in CRC patients with and without distant metastases

Mutations in 48 cancer driver– and cancer pathway–related genes (table S2) were investigated using data from the Cancer Genome Atlas (TCGA) (cohort 1) (*22*). In primary tumors from patients with (M1) or without (M0) metastases, cancer genes showed a similar profile (Fig. 1A and table S2) and frequency of mutation for each of the exons tested (fig. S1A). These cancer genes were also analyzed in a second cohort (cohort 2) using next-generation sequencing. Patients presented with a mean of 4 ± 2 mutations: *APC*, *KRAS*, *BRAF*, and *TP53* were mutated in 36.6, 41.5, 17, and 49.6% of the cohort, respectively. The overall pattern of mutations detected in M1 and M0 patients was highly

[1]INSERM, UMRS1138, Laboratory of Integrative Cancer Immunology, F-75006 Paris, France. [2]Université Paris Descartes, Sorbonne Paris Cité, UMRS1138, F-75006 Paris, France. [3]Sorbonne Universités, UPMC Univ Paris 06, UMRS1138, Centre de Recherche des Cordeliers, F-75006 Paris, France. [4]AstraZeneca, Cambridge CB4 OWG, UK. [5]Institute of Human Genetics, Medical University of Graz, Graz, Austria. [6]Department of Medicine, University of Erlangen-Nuremberg, Erlangen, Germany. [7]Assistance Publique–Hopitaux de Paris, Department of General and Digestive Surgery, Hôpital Européen Georges Pompidou, Paris, France. [8]Assistance Publique–Hopitaux de Paris, Department of Immunology, Hôpital Européen Georges Pompidou, Paris, France. [9]MedImmune Ltd., Cambridge CB21 GGH, UK.
*These authors contributed equally to this work.
†Corresponding author. E-mail: jerome.galon@crc.jussieu.fr

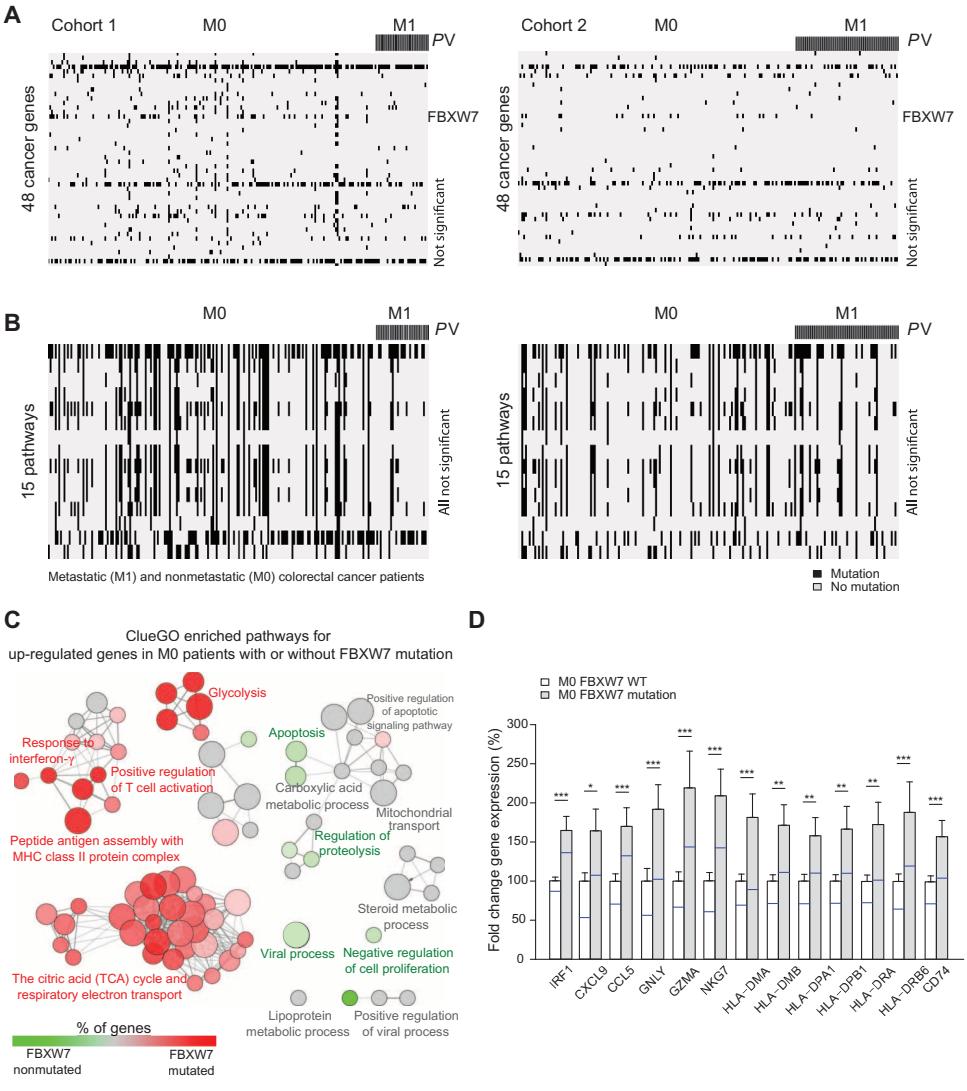

Fig. 1. Mutations of known cancer genes in metastatic CRC patients. (**A** and **B**) Mutations of 48 cancer genes (table S2) (A) and of 15 cancer pathways (table S3) (B) in CRC patients with (M1) or without (M0) metastasis from cohorts 1 and 2. M1 patients and mutations are shown in black; nonmutated genes or pathways are in gray. Genes and pathways are sorted alphabetically. A pathway was considered mutated if at least two of the associated genes were mutated. Fisher's exact test was used to compare mutations between M0 and M1. (**C**) Significantly differentially expressed genes ($P < 0.05$) in M0 patients with or without FBXW7 mutation were investigated in cohort 1 (RNA-Seq) using CluePedia. From these genes, the 167 up-regulated and 278 down-regulated genes having $\Delta > 5$ were analyzed with ClueGO. Enriched pathways are shown as nodes interconnected based on the κ score. The color gradient shows the proportion of genes up-regulated in FBXW7-mutated (red) and nonmutated (green) M0 patients associated to each of the pathways. Equal proportion is shown in gray. The size of the nodes shows the term significance (right-sided hypergeometric test, Bonferroni step-down correction). (**D**) Up-regulated immune genes in FBXW7-mutated patients (C). Bar charts represent means ± SEM, and the median expression is shown in blue. Figure S1 extends Fig. 1.

similar (table S2), confirming the results observed in cohort 1 (Fig. 1A). None of the 48 major cancer genes were more frequently mutated in M1 patients. Similarly, no difference was found in the frequency of mutations for each target region tested (fig. S1A) or for the 15 cancer pathways investigated (Fig. 1B and table S3). As previously described (*23*), BRAF mutations occurred more often in tumors of the right colon compared to other colonic regions or rectum and affected more women than men (*24*). Mutations in the other cancer genes were not associated with the tumor localization or with other clinical parameters as the extent of the tumor, lymphatic node invasion, and UICC-TNM (International Union Against Cancer tumor-node-metastasis) status (table S4). None of these mutations, nor the sum of the mutations from these genes, were significantly associated with the disease-specific survival of the patients, as illustrated for *BRAF* (fig. S1C). *FBXW7* mutations were significantly more frequent in M0 patients in cohort 1, and data were validated in cohort 2. ClueGO (*25*) and CluePedia (*26*) were used to find which genes are up-regulated in M0 patients with or without *FBXW7* mutations and which is their biological role. Genes involved in response to interferon-γ, positive regulation of T cell activation (*IRF1*, *CXCL9*, *CCL5*, *GNLY*, *GZMA*, and *NKG7*), and major histocompatibility complex (MHC) class II–related pathways (*HLA-DMA*, *HLA-DMB*, *HLA-DPA1*, *HLA-DPB1*, *HLA-DRA*, *HLA-DRB6*, and *CD74*) as well as in the citric acid cycle or glycolysis-related terms were up-regulated in *FBXW7*-mutated patients (Fig. 1, C and D). In comparison, M0 patients without *FBXW7* mutation had up-regulated genes involved in apoptosis, regulation of proteolysis, and negative regulation of cell proliferation.

Next, the chromosomal instability (CIN) of CRC tumors was analyzed using array comparative genomic hybridization (aCGH). Amplifications and deletions of the cancer genes were compared between M0 and M1 patients (Fig. 2A). *VHL* and *FBXW7* were significantly deleted more often in M1 compared to M0 in cohorts 1 and 2, respectively. Additionally, amplification and deletion scores were calculated for every gene within each cohort (described in Materials and Methods). The genomic profiles of patients from cohorts 1 and 2 were remarkably similar (fig. S2). As expected, we identified multiple gains and losses of chromosomal regions that have previously been reported in CRC, including the gain of 8q and the loss of 8p (*27*). The overall pattern of chromosome alteration in the primary tumors from M1 and M0 patients displayed high congruency (Fig. 2B). Amplifications of only 16 genes from chromosomes 13 and 20 were found to be significantly overrepresented in M1 patients compared to M0 for both cohorts. In comparison, deletions of 339 genes were significantly overrepresented in M1 compared to M0 patients, with most of these deletions located on chromosomes 8 and 18. Additional deleted genes were located in chromosomes 4, 10, 12, 13, and 22 (fig. S2B).

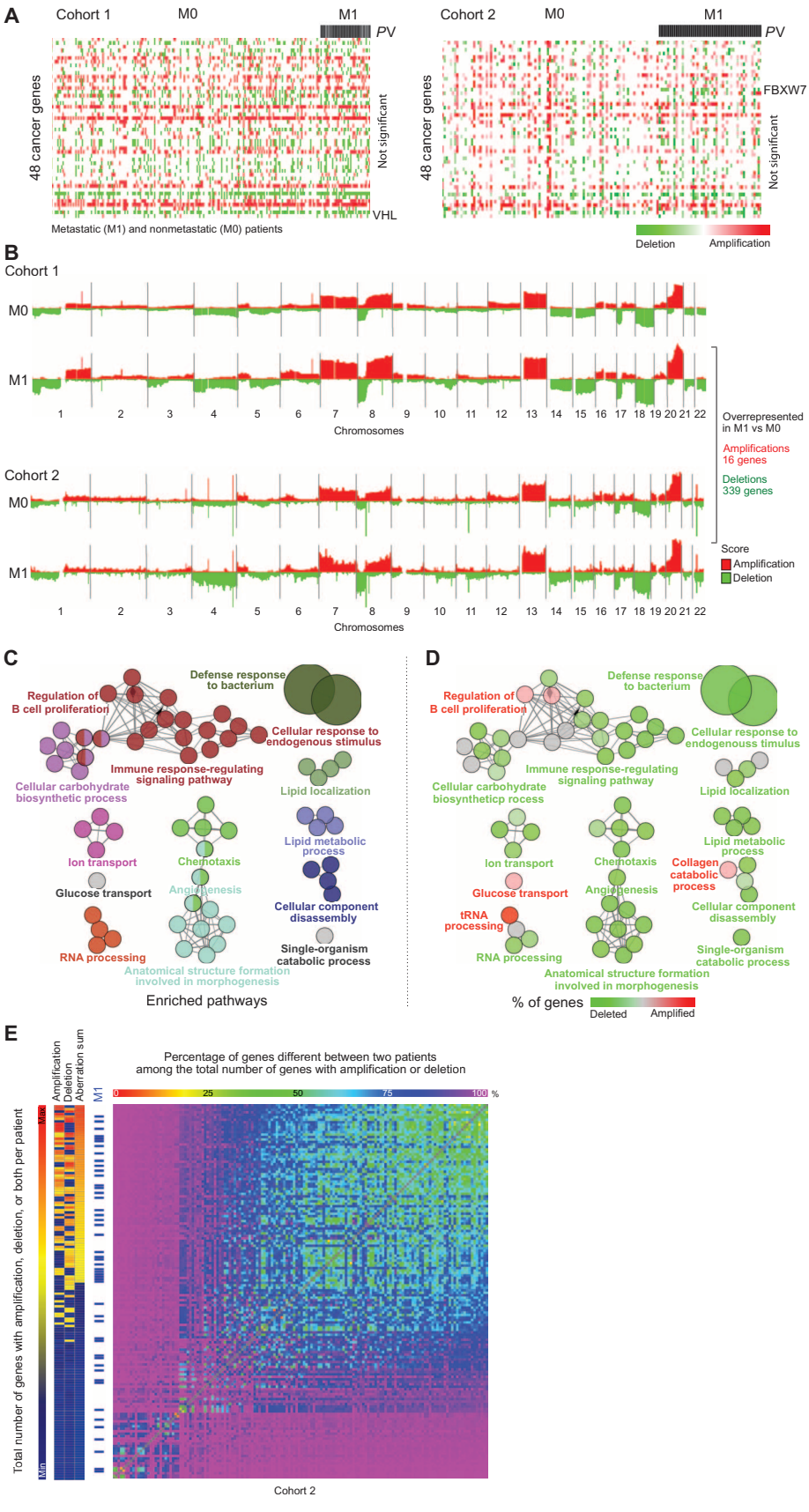

Fig. 2. Genomic alterations in metastatic CRC patients. (**A**) Amplifications (red) and deletions (green) of 48 cancer genes in M0 and M1 (black) patients from cohorts 1 and 2. No aberrations are shown in white. Genes showing different aberration profiles are highlighted. (**B**) aCGH profile in M0 and M1 patients. The frequency and the amplitude of the gain or loss of each gene were used to calculate an amplification (red) or deletion (green) score for M0 and M1 patients. The X and Y chromosomes were excluded. Fisher's exact test was applied. Functional analysis of the significantly amplified ($n = 16$) or deleted ($n = 339$) genes using ClueGO (**C**). Nodes represent enriched pathways grouped based on shared genes and linked based on the κ score. The size of the node shows the term significance (right-sided hypergeometric test, Bonferroni step-down correction). (**D**) Distribution of the genes on pathways. The color gradient shows the proportion of amplified (red) and deleted (green) genes associated to each pathway. Equal proportion is shown in gray. (**E**) Copy number heterogeneity matrix. Heat map with percentage of genes having different amplifications and deletions among all genes with alteration between two patients for all the patients from cohort 2. Minimum and maximum difference is shown with a rainbow color code. Patients compared with themselves are shown in gray. The number of amplifications, deletions, and total aberrations is shown for each patient (left). The counts are represented with a color gradient ranging from dark blue (minimum = 0) to red (maximum = 20,424). On the *y* axis, M1 patients are shown in blue. Figure S2 extends Fig. 2.

ClueGO and CluePedia (*25*, *26*) analysis of the overrepresented amplified and deleted genes (table S5) revealed the biological role of these altered cancer genes (Fig. 2C). The amplified genes were associated with glucose transport, transfer RNA (tRNA) processing, and regulation of B cell proliferation (Fig. 2D), whereas deleted genes were involved in immune-related pathways, defense response, angiogenesis, metabolic processes, and morphogenesis. Specifically, there was a significant increase in M1 patients with deletions in members of the defensin family, cytotoxic proteins involved in host defense (fig. S2C). Out of the significantly overrepresented genes, only *SMAD2* and *SOX17* have been previously reported as cancer genes (table S6) (*28*, *29*). Although the genomic patterns across the cohorts were similar, there were marked differences at the individual level, where all tumors harbored different sets of gains and losses. Genes with copy number aberrations were compared in all patient pairs, and the percentage of altered genes was displayed in a copy number heterogeneity matrix (Fig. 2E). There was considerable heterogeneity among tumors, and the mean

number of genes amplified or deleted was 3920 and 2750 per patient, respectively. The mean percentage of differential gene alterations between two patients was 82%. Remarkably, tumors from some individuals, including M1 patients, showed no evidence of CIN (fig. S2D). The maximum numbers of deletions or amplifications were observed in a total of only two or eight patients, respectively (fig. S2E). The copy number changes across the tumor genome were personalized for each patient.

Immune-related gene expression discriminates patients with and without distant metastases

The expression of the 48 cancer genes was investigated in relation to the presence of synchronous metastasis for cohort 1. Surprisingly, most of the genes had similar expression levels regardless of M0 or M1 status, and only *BRAF*, *EGFR*, *JAK2*, and *SRC* reached statistically significant differences between M1 and M0 patients (Fig. 3A). To validate this observation, we analyzed the cancer genes using Affymetrix arrays in cohort 3 (Fig. 3B). Concordant results were observed in both cohorts 1 and 3. *JAK2* was the only gene differentially expressed in both cohorts. Additionally, the expression of cancer genes known to be involved in metastasis process, tumor progression, and WNT pathway (table S6) was investigated in cohort 1. Surprisingly, most of the metastasis-related genes had similar expression levels regardless of M0 or M1 status, and only *PTP4A3*, *PTPRC*, *CXCR4*, and *VEGFA* reached statistically significant differences between M1 and M0 patients (fig. S3A). To validate this observation, we analyzed the tumor-related genes using real-time quantitative polymerase chain reaction (qPCR) in cohort 3. The qPCR results confirmed the gene expression results from cohort 1 and showed no difference in tumor-related gene expression between M0 and M1 patients, except for two genes: *CSF1* and *MMP9* (fig. S3B). The expression of *JAK2*, *SMAD2*, and *FZD1* was slightly decreased in tumors with synchronous metastases, whereas *DKK1* and *TCF7* levels were increased. However, these changes in expression levels did not reach statistical significance. Equivalent results were obtained for genes known to be associated with the tumor progression as well as a larger panel of genes involved in the WNT pathway (table S6)

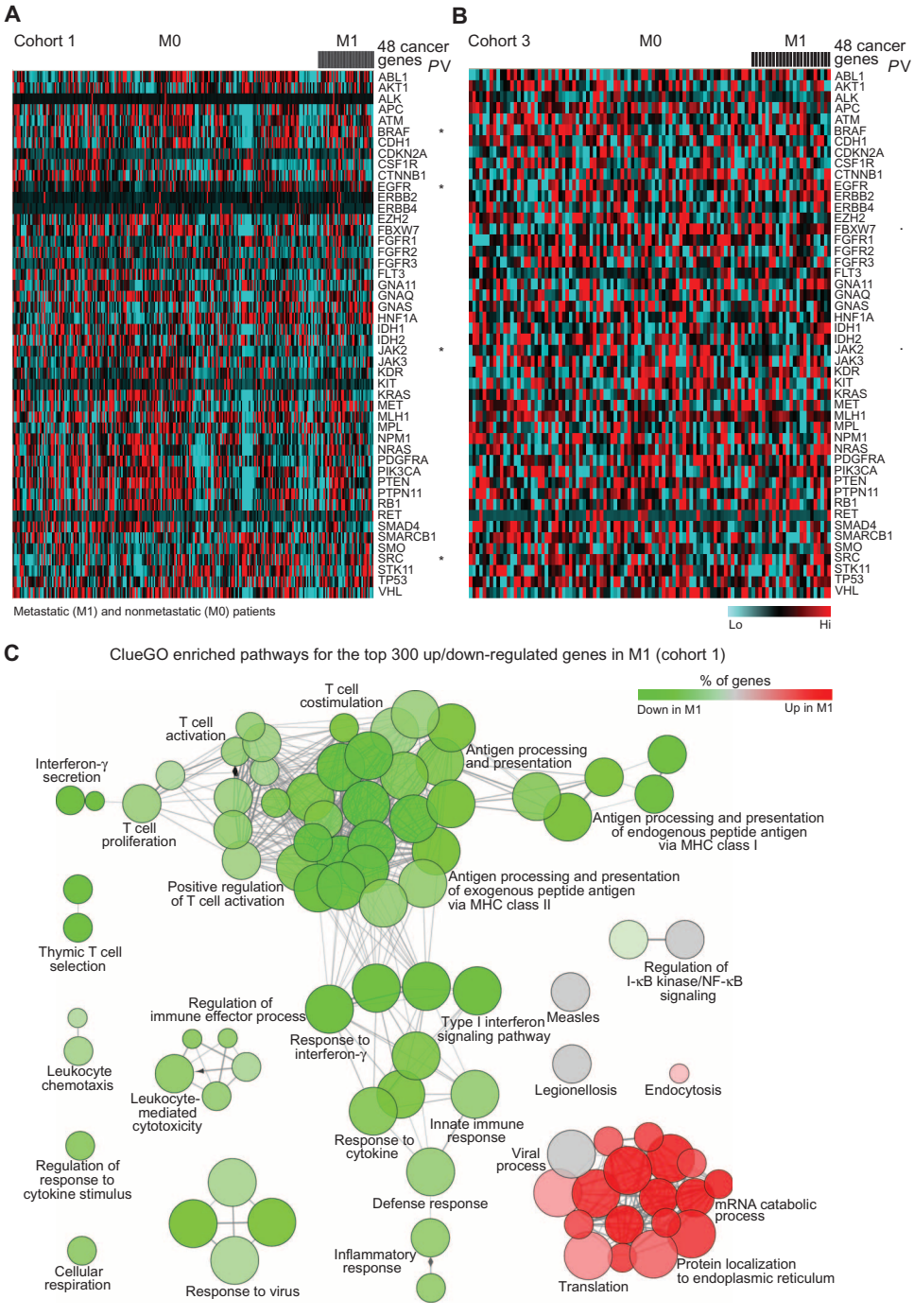

Fig. 3. Cancer-related gene expression in metastatic CRC patients. (**A** and **B**) Expression of cancer genes measured with RNA-Seq in cohort 1 (A) and Affymetrix microarrays in cohort 3 (B). M1 patients are marked in black. Minimum (Lo) and maximum (Hi) normalized expression scaling from −1 to 1 for both cohorts are shown in blue and red, respectively. Genes significantly differentially expressed between M0 and M1 are marked (*$0.01 \geq P < 0.05$, $0.05 \geq P < 1$). (**C**) Significantly differentially expressed genes ($P < 0.05$) in M1 versus M0 were investigated in cohort 1 (RNA-Seq) using CluePedia (*26*). From these genes, the top up-regulated ($n = 300$) and down-regulated ($n = 300$) genes having the highest expression level difference between M1 and M0 were analyzed with ClueGO. Enriched pathways and functions are shown as nodes interconnected based on the κ score. The color of the node shows the proportion of up-regulated (red) and down-regulated (green) genes in M1 associated to each of the pathways. Equal proportion is shown in gray. The size of the nodes shows the term significance (right-sided hypergeometric test, Bonferroni step-down correction).

also analyzed by qPCR in cohort 3 (fig. S3, C and D). Strikingly, most genes had similar expression in tumors with and without metastases and were therefore not considered to be associated with the presence of metastasis.

Because no major differences were found in cancer genes based on metastatic status, a comprehensive analysis of RNA-Seq expression data from primary tumors from cohort 1 was performed to identify differentially expressed genes. The 300 significantly up- and down-regulated genes having the highest expression level difference between M0 and M1 patients were investigated (Fig. 3C). Genes down-regulated in M1 patients were involved in numerous immune functions, including defense response; interferon-γ secretion; response to interferon-γ; type I interferon signaling pathway; antigen processing and presentation; MHC class I and II regulation; leukocyte-mediated cytotoxicity and chemotaxis; T cell activation, proliferation, and costimulation; response to cytokines; viral response; innate immunity; and inflammation (Fig. 3C). Genes up-regulated in M1 patients were involved in translation, protein localization to the endoplasmic reticulum, mRNA catabolic process, and endocytosis. These findings were validated in cohort 3 using DNA microarray data (fig. S4A).

This analysis performed in two independent cohorts underlined the potential importance of immune-related genes in predicting the metastatic status of CRC patients. Further investigation of immune-related genes by real-time qPCR in cohort 3 confirmed that patients with metastases had decreased expression of many immune genes including those regulating T helper 1 (T_H1) response, lymphocyte cytotoxicity, and activation, as well as MHC class II–related genes (Fig. 4, A and B, and fig. S4B). The only other innate immune gene reaching a statistically significant increase in metastatic patients was the macrophage marker *CD68* (Fig. 4B). Patients without metastasis had a significant increase in expression of T_H1-related (*IL12B*, *TBX21*, *IFNG*, *CCR5*, and *STAT1*), immune cytotoxicity–related (*GNLY*, *CD8A*, *GZMA*, *GZMH*, and *GZMK*), and MHC class II–related (*HLA-DMA*, *HLA-DMB*, *HLA-DOA*, *HLA-DOB*, *DPA1*, and *CD74*) genes and increased expression of *IL12RB2* and *GZMB* compared to patients having metastases at the time of diagnosis. Remarkably, examination of primary tumors of patients who developed metachronous metastases years after diagnosis also showed decreased expression of the same immune genes (Fig. 4B). Thus, in contrast to copy number patterns and cancer gene expression, adaptive immune gene expression appears to discriminate between patients with or without metastases.

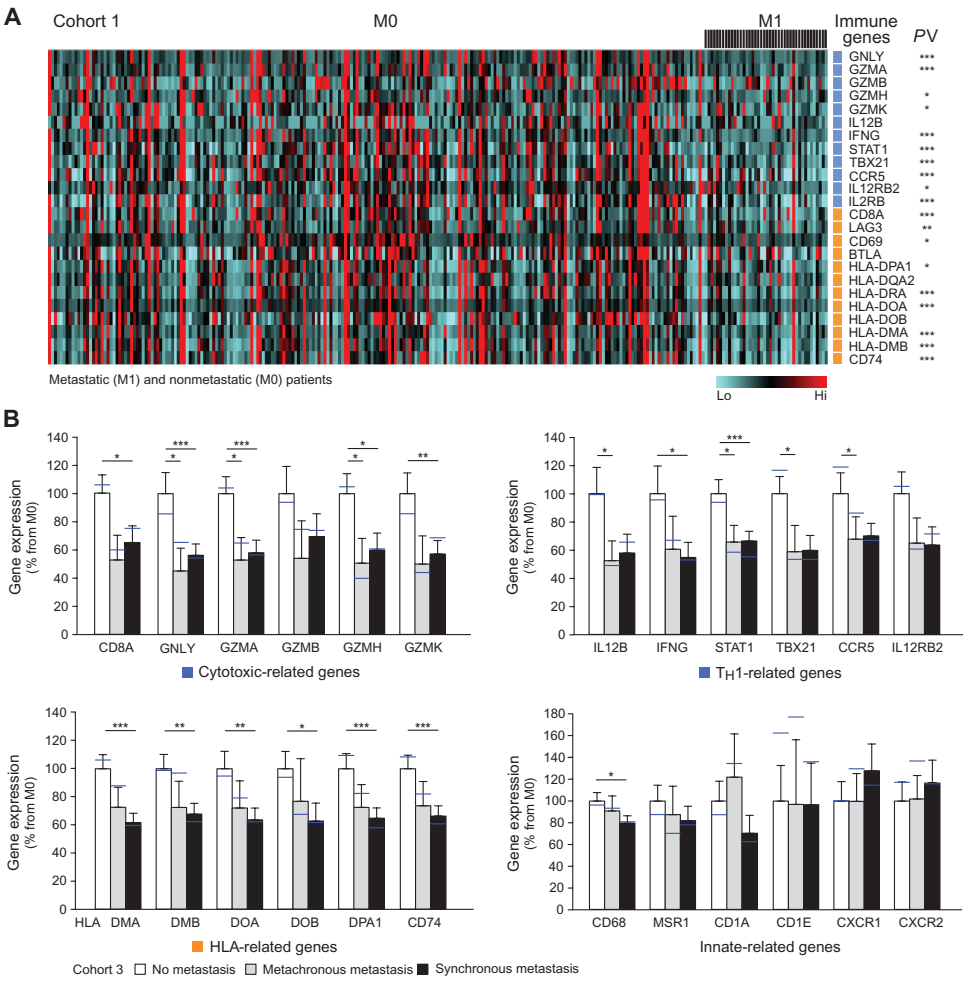

Fig. 4. Immune-related gene expression in metastatic CRC patients. (**A**) Expression of immune genes (cytotoxic-, T_H1-, and HLA-related) was investigated in cohort 1 (RNA-Seq). M1 patients are marked in black. Minimum (Lo) and maximum (Hi) normalized expression scaling from −1 to 1 are shown in blue and red, respectively. Genes significantly differentially expressed between M0 and M1 are marked (***$P < 0.005$, **$0.005 \geq P < 0.01$, *$0.01 \geq P < 0.05$). (**B**) Expression of immune genes (cytotoxic-, T_H1-, HLA-, and innate-related) measured by qPCR in CRC patients from cohort 3. Bar charts represent the relative expression compared to M0 ± SEM. Patients without metastasis and with metachronous or synchronous metastasis are shown in white, gray, and black, respectively. A parametric or nonparametric test was applied based on Shapiro normality test (***$P < 0.005$, **$0.005 \geq P < 0.01$, *$0.01 \geq P < 0.05$).

LVD within the invasive margin and immune cytotoxicity is decreased in patients with distant metastases

To determine the potential contribution of blood and lymphatic vasculature to metastatic progression, we analyzed BVD and LVD in primary CRC tumors using immunohistochemistry for cohorts 3 and 4 (Fig. 5A). There was no significant difference in BVD between M0 and M1 patients (Fig. 5B), even when density was further defined by location in the center (CT) or the invasive margin (IM) of the tumor (fig. S5A). In contrast, the LVD was significantly decreased in patients with metastases (Fig. 5B). This decrease in LVD was specific for the IM and not the CT in primary tumors of metastatic patients (Fig. 5, C and D). Similar results for BVD and LVD were observed for cohort 4 (Fig. 5, E to G, and fig. S5B). Additionally, the early metastatic invasion of tumor cells inside lymphatic vessels was visualized (fig. S5C).

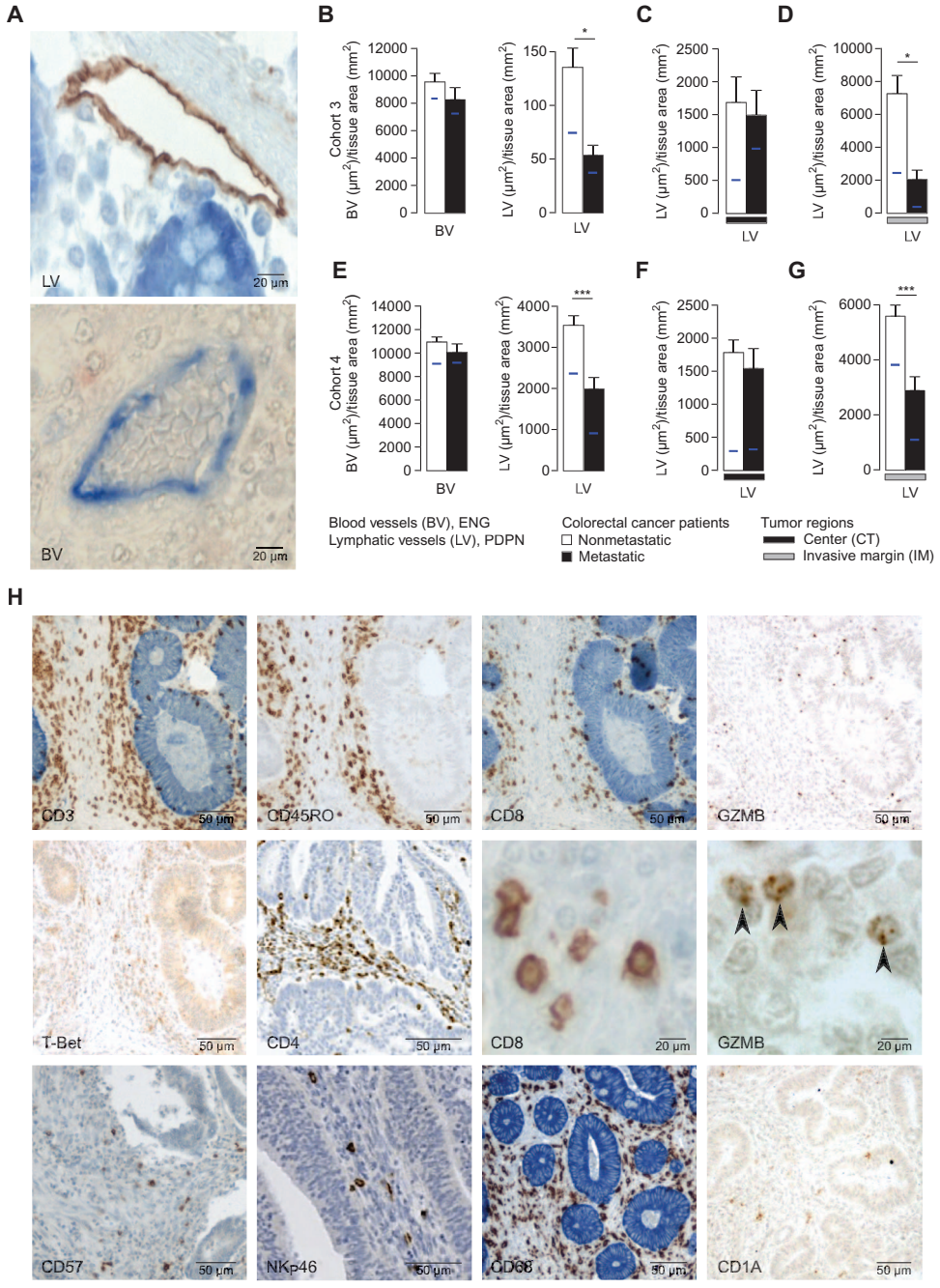

Fig. 5. Blood vessel (BV) and lymphatic vessel (LV) density in metastatic CRC patients. (**A** and **H**) Representative examples of blood vessel, lymphatic vessel, total T cell (CD3), T helper cell (CD4), T_H1 cell (T-Bet), memory cell (CD45RO), cytotoxic cell (CD8, GZMB, CD57), NK cell (NKp46), macrophage (CD68), and immature dendritic cell (CD1A) staining of a CRC tissue microarray (TMA). Antibodies to endoglin (ENG; CD105) and podoplanin (PDPN) were used for blood and lymphatic vessels, respectively. The density was recorded as μm^2 of blood vessels/mm^2 of tissue and μm^2 of lymphatic vessels/mm^2 of tissue using a dedicated image analysis workstation (Spot Browser ALPHELYS). Bar charts represent means ± SEM of endothelial area of blood and lymphatic vessels in tumors from cohort 3 (B to D) and cohort 4 (E to G). (**B** and **E**) Blood and lymphatic vessel density in M0 and M1 patients. (**C** and **F**) Lymphatic vessel density in the center of the tumor (CT; black). (**D** and **G**) Lymphatic vessel density in the invasive margin (IM; gray). The density in M0 and M1 is shown in white and black, respectively. A parametric or nonparametric test was applied based on Shapiro normality test (***$P < 0.005$, **$0.005 \geq P < 0.01$, *$0.01 \geq P < 0.05$).

Next, we determined whether intratumoral immune cell density correlates with the metastatic status. Intratumoral infiltrate with total T cells (CD3), T helper cells (CD4), T_H1 cells (T-Bet), memory cells (CD45RO), cytotoxic cells (CD8, GZMB, CD57), natural killer (NK) cells (NKp46), macrophages (CD68), and immature dendritic cells (CD1A) was investigated in cohorts 3 and 4 (Fig. 4H and fig. S5, D and E). The density of CD3, CD8, CD57, GZMB, CD45RO, and T-Bet lymphocytes was instead significantly decreased in both the CT (Fig. 6A) and the IM of metastatic patients (Fig. 6B). This discrepancy between metastatic and nonmetastatic patients was particularly notable for the cytotoxic molecule GZMB ($P < 0.00001$) (Fig. 6, A and B). These results were confirmed in cohort 3 (fig. S6, A and B). Triple stainings [CD8/GZMB/cytokeratin (CK) and NKp46/GZMB/CK] illustrate most $GZMB^+$ cells being CD8 cytotoxic cells (fig. S5, D to F). Macrophage (CD68) density showed a significant decrease in the CT of metastatic patients. In contrast, no significant differences were observed with NK cells (NKp46) or immature dendritic cells (CD1A) (Fig. 6, A and B, and fig. S6).

Distant metastasis is a consequence of decreased $PDPN^+$ lymphatic vessels and cytotoxic lymphocytes

The presence of metastasis is associated with major changes in the tumor microenvironment and immune infiltrate; however, it remains unclear whether the development of metastases is a cause or a consequence of a specific immune contexture (*21*). To explore this phenomenon, we evaluated patients with signs of early-distant metastatic invasion, as characterized by perineural invasion (PI) or vascular emboli (VE), for immune infiltrates within the tumor. No significant differences were found in cell densities in the CT between patients with (PI^+) or without (PI^-) perineural invasion for CD3, CD8, CD57, T-Bet, CD45RO, GZMB, CD68, CD1A, CD4, and NKp46 (Fig. 6C and fig. S6C). Similar results were observed in the CT for patients with (VE^+) or without (VE^-) vascular emboli (Fig. 6E). In contrast, in the IM region, PI^+ patients had a significant decrease in density of CD3, CD8, CD45RO, and

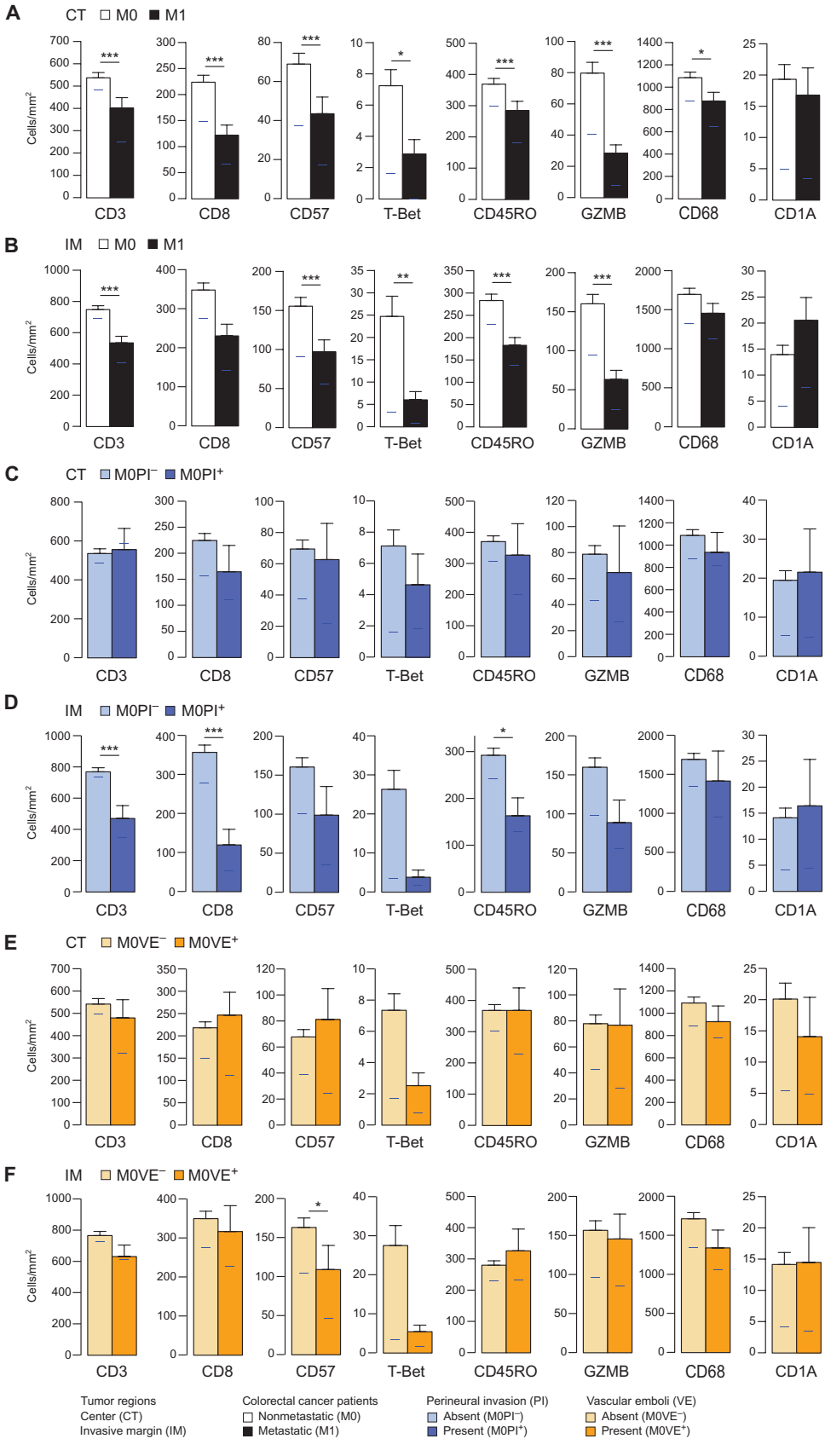

Fig. 6. Immune cell density in metastatic CRC patients. Immune cell infiltrates in patients from cohort 4 measured by TMA. T cells (quantified with marker CD3), cytotoxic T cells (CD8, CD57, and GZMB), T_H1 cells (T-Bet), memory T cells (CD45RO), macrophages (CD68), and immature dendritic cells (CD1A) were quantified by immunohistochemistry. (**A** to **F**) The density was calculated as the number of positive cells/mm^2 of tissue in the center of the tumor (CT) (A, C, and E) and in the invasive margin (IM) (B, D, and F). Immune densities in patients with (M1) or without metastasis (M0) (A and B) are shown in black and white, respectively. Immune densities in M0 patients with (PI$^+$) or without (PI$^-$) perineural invasion (C and D) or having (VE$^+$) or not (VE$^-$) vascular emboli (E and F) are shown in blue, light blue, orange, and light orange, respectively. Bar charts represent means ± SEM immune density. A parametric or nonparametric test was applied based on Shapiro normality test (***$P < 0.005$, **$0.005 \geq P < 0.01$, *$0.01 \geq P < 0.05$).

CD4 (Fig. 6D and fig. S6D) and a decrease of CD57, T-Bet, and GZMB. VE$^+$ patients had a significant decrease in density of CD57 and decrease of T-Bet, CD3, CD8, GZMB, and CD4 in the IM (Fig. 6F and fig. S6D), suggesting changes in lymphocytic infiltration and function at the earliest stages of metastatic progression.

The protective role of cytotoxic T cells for CRC progression was investigated using an endoscopic orthotopic tumor model to which C57Bl/6 mice were exposed. MC38 CRC mouse cell line was injected endoscopically into the colonic submucosa of C57Bl/6 mice with or without CD8 depletion, and tumor growth was monitored weekly (fig. S6F). The tumor mass that formed in the intestinal wall from injected tumor cells was continuously increasing in time (fig. S6G). Orthotopic MC38 tumors had a significantly accelerated growth in CD8-depleted C57Bl/6 mice, indicating an important functional immune control in a CRC mouse tumor model.

Hallmarks of the metastatic process progression are the combined decrease of PDPN$^+$ lymphatic vessels and immune cytotoxicity

Because both high lymphatic vessel and cytotoxic lymphocyte densities appear to be independent markers that significantly

correlate with decreased metastatic potential, the combined analysis of LVD, BVD, and immune cell densities was performed to determine whether together these are superior biomarkers of metastatic potential. The cumulative frequency pyramid matrices were used to represent the frequency of metastasis in groups of patients based on location (CT and IM) of LVD, BVD, and immune cell densities (Fig. 7A and fig. S7). Whereas BVD had no effect on metastasis, the combination of cytotoxic lymphocyte density from the CT (GZMB-CT) and the LVD measured in the IM (PDPN-IM) showed a significant correlation to metastatic status (Fig. 7A). Decreased densities of LVD-IM or GZMB-CT were highly associated with metastatic frequency from 9 to 31% and from 0 to 47%, respectively (Fig. 7A). As an example, analysis of the cohort with low density (Lo) of PDPN-IM and GZMB-CT (right bottom quadrant) revealed that this combination is associated with a high frequency of synchronous metastasis. In contrast, only 8% of the patients with high (Hi) levels of GZMB had metastases. The rate of metastasis increased in a gradient ranging from 8 to 49% in direct correlation with decreasing GZMB density (Fig. 7A). Patients with low densities of GZMB and PDPN (LoLo) were significantly overrepresented in M1 compared to M0 patients (Fig. 7B). Most importantly, patients with GZMB and PDPN HiHi densities showed a significant prolongation of OS (Fig. 7B).

The quantification of T cells and cytotoxic T cells (CD3 and CD8) in the CT and IM of CRC tumors has been defined as the Immunoscore (*30*). Immunoscore stratifies patients based on immune cell densities and locations in the primary tumor on a scale of I0 to I4, where patients with high densities of all markers in all locations are scored as I4 and patients with low densities for all markers in all locations are I0. Immunoscore low (I0) tumors were significantly overrepresented in M1 compared to M0 patients (Fig. 7C). For both M0 and M1 patients, a low (I0) or intermediate (I int) Immunoscore was associated with a shorter OS compared to patients with a high Immunoscore (I4) (Fig. 7C). Thus, even among stage IV patients having distant metastases, Immunoscore significantly identifies patients with the longest OS (I4: 65% OS at 5 years). These data show that high Immunoscore, LVD-IM, and GZMB-CT are significantly associated with the absence of metastases, and combining these parameters may allow for accurate prediction of synchronous metastasis.

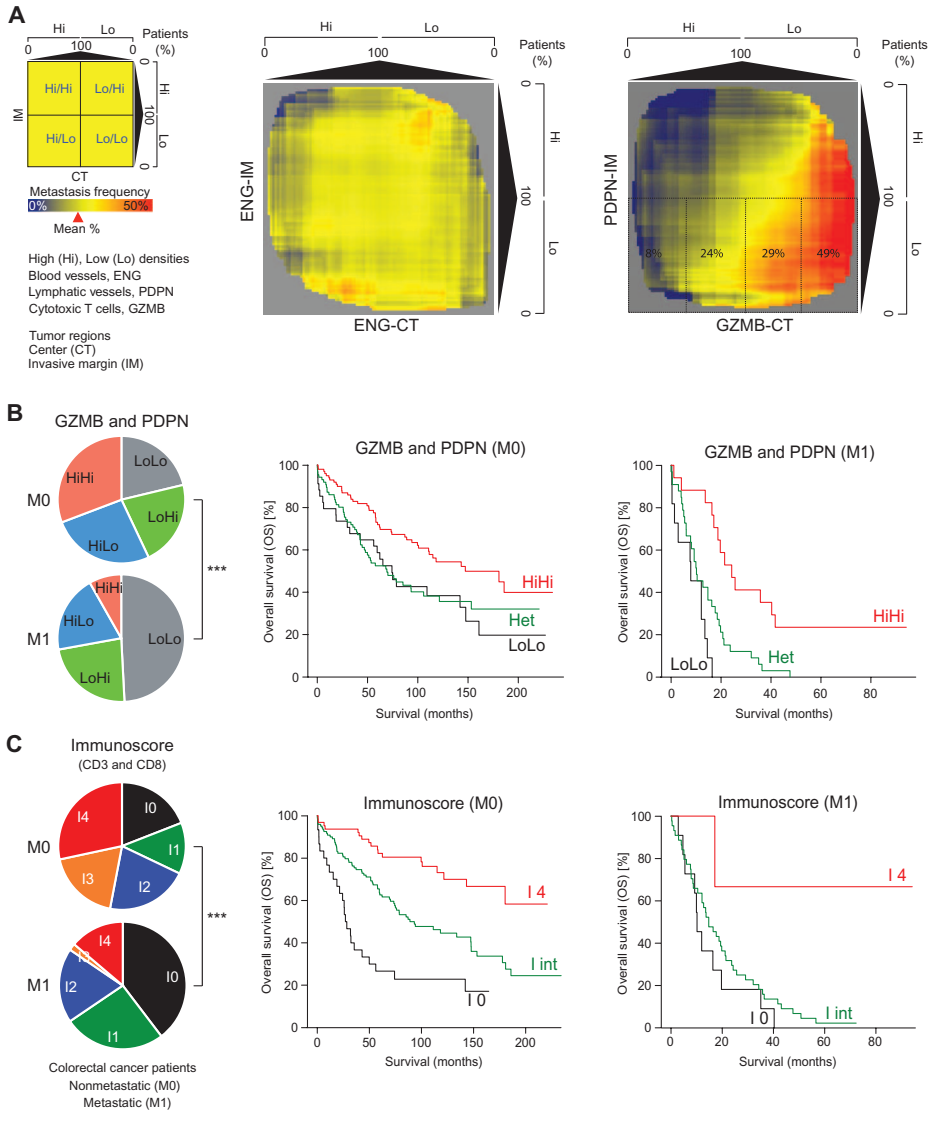

Fig. 7. The impact of the density of tumor microenvironment components on the metastasis. (**A**) Cumulative frequency pyramids based on the frequency of the synchronous metastasis in patient groups with different densities of cytotoxic (GZMB), blood (ENG), or lymphatic vessel (PDPN) markers from CT and IM (cohort 2). The top left and bottom right pyramid corners correspond to patients with high and low densities of both markers, respectively. All patients (100%) are represented in the center of the pyramid. Metastasis frequency (mean, 23%) is shown with a color gradient (blue, low to red, high). Mean metastasis rate within each lower quadrant is shown. (**B**) Frequency of patient groups defined based on the high (Hi) or low (Lo) density of GZMB in CT and PDPN in IM in M0 and M1 (median *P* value cutoff): LoLo (gray), LoHi (green), HiLo (blue), HiHi (red). Kaplan-Meier estimates of overall survival (OS) according to the GZMB-CT and PDPN-IM densities in M0 and M1 patients (minimum *P* value cutoff). HiLo and LoHi groups were pooled (Het). (**C**) Frequency of Immunoscore groups in M0 and M1 (median *P* value cutoff). Immunoscore summarizes the high (Hi) density of CD3 and CD8 in CT and IM: I0 (0Hi, black), I1 (1Hi, green), I2 (2Hi, blue), I3 (3Hi, orange), I4 (4Hi, red). Kaplan-Meier for OS for Immunoscore in M0 and M1 (minimum *P* value cutoff). I1, I2, and I3 were pooled (I int). See also fig. S7.

DISCUSSION

Here, we addressed three major questions. First, are differences in tumor genotype and transcription profile associated with distant metastases? Second, are microenvironmental factors, specifically blood and lymphatic vascularization and immune phenotype, associated with distant metastases? Last, are distant metastases a cause or

a consequence of these differences in tumor cells, vascularization, or immunity in the primary tumor?

Despite numerous studies, the metastatic process remains unclear, although several hypotheses could be proposed. The first possibility is that there is a defined tumor cell–intrinsic phenotype, which can be detected in the bulk tumor that predisposes toward metastasis. This hypothesis is not supported by our data, which showed a minimal impact of primary tumor CIN, cancer-related mutations, and tumor-related gene expression on the presence of metastases. The second hypothesis is that only a small number of tumor cells are able to metastasize, and their genomic alterations could not be detected. Here, integrative cancer immunology approaches allowed us to have a comprehensive view of the tumor CIN, tumor gene mutation pattern, gene expression pattern, and the immune system's evolution with tumor dissemination to distant metastasis. We perform a comprehensive analysis of both tumors and microenvironment factors, including blood and lymphatic vessels and many immune cell subpopulations, in relation with synchronous distant metastasis. Strikingly, this comprehensive analysis revealed that the main parameters associated with dissemination to distant metastasis are immune-related and not tumor-related. A limitation of the study relates to the possibility that rare cancer stem cells may be in part responsible for metastasis invasion. The cancer stem cell hypothesis posits that a distinct subset of specialized cells retains the capacity to self-renew and continuously populates the tumor and the metastasis. The technologies used here may not allow their detection. However, major immune changes were demonstrated, emphasizing the importance of the preexisting immunity, independently of the possible implication of cancer stem cells. Specific gene expression has been reported in metastatic tumor cells from metastases in different cancer types (*29*, *31*), which may indicate the presence of cancer stem cells, considered to be moderators of tumor progression and metastasis (*32*). However, this hypothesis is contradicted by results showing the genetic similarity between primary CRC and paired metastatic tumor cells (*5*). Considerable genetic heterogeneity has also been observed among cells capable of initiating metastasis (*4*), and it was reported that primary tumors contain a mix of geographically distinct subclones before clinical manifestation of metastatic disease (*33*, *34*). The features of the metastasis-promoting subclones have yet to be discerned with no consistent genetic signature identified (*33*, *34*), although some candidate genes for CRC cancer stem cells have been proposed (*35*). Mutations found in metastases were not specific because they were already present in the matched primary carcinoma (*5*). Our study also shows a remarkably similar mutation frequency pattern between patients with or without metastases. Thus, it is unlikely that any of these mutations in "cancer driver mutation" genes are particularly responsible for driving metastasis.

No cancer-associated genes or pathways were associated with M stage. Instead, mutations of *FBXW7* were associated with the absence of metastasis. Recently, the analysis of 1519 CRC patients revealed that in early-stage (I/II) CRC patients, the mutant *FBXW7* was more common than the wild-type *FBXW7* (*36*). It was demonstrated that *FBXW7* inhibits cancer metastasis in a non–cell-autonomous manner through accumulation of NOTCH and consequent transcriptional activation of *Ccl2* (*37*). *FBXW7* also attenuated inflammatory signaling by down-regulating C/EBPδ and its target gene *Tlr4*, and *FBXW7* depletion alone was sufficient to augment proinflammatory signaling in vivo (*38*). Thus, through increased proinflammatory signaling, *FBXW7* mutation could increase T cell proliferation and antigen presentation functions. This could be one of the mechanisms leading to increased adaptive immunity and protection against metastasis.

In contrast to a model of cell-autonomous genomic alterations driving metastasis, it has been proposed that metastatic traits are acquired through exposure to paracrine signals received from the tumor microenvironment (*39*). In pancreatic cancer, genomic data did not reveal the selective pressures within the primary carcinoma that lead to mutations resulting in dissemination of tumor cells (*34*). Therefore, an appealing alternate hypothesis is that the selective pressure may occur in the microenvironment, in particular via the immune phenotype.

We have shown a strong association between intratumoral immune cytotoxicity and the metastatic process. In addition, we have observed a significant decrease in lymphocyte densities (CD3, GZMB, CD8, T-Bet, CD57, and CD45RO) in the primary tumors of patients with metastases. We further demonstrated the functional relevant antitumor cytotoxic response using an endoscopic orthotopic mouse model. MC38 tumors had a significantly accelerated growth in CD8-depleted C57Bl/6 mice in comparison to wild-type mice. These results are in concordance with previous reports, showing that in mice, the disruption of the T_H1 response was associated with increased metastatic disease, where cytotoxic T lymphocytes were the major cell type preventing distant synchronous metastases (*40*). We observed that high Immunoscore, high-density LVD at the IM, and high density of cytotoxic cells (GZMB) correlated with a decreased likelihood of metastasis (Fig. 6). The LVD in the IM also correlated with the lymphocyte density in the CT and IM. These lymphatic vessels may increase the immune response by facilitating the transport of tumor antigens alone or via antigen-presenting cells to draining lymph nodes to initiate immune priming. Thus, a combined low density of lymphatic vessels and effector T lymphocytes may license tumor cells to metastasize.

We recently described mechanisms resulting in changes of specific immune cell densities within the tumor and the importance of local active lymphocyte proliferation, mediated by IL15, to prolong patient survival (*41*). An integrative study of immune parameters revealed the immune landscape in human CRC and the major hallmarks of the microenvironment associated with tumor progression within the primary tumor (*14*, *42*). The immunogenic neo-epitopes arising from passage mutations have been recently characterized (*43*), and the relationship between immunogenicity and immunophenotype was underlined (*44*). Here, we characterized tumor and microenvironmental parameters associated with synchronous metastases, and compared them to early metastatic events and the occurrence of metachronous metastases. We have previously proposed the concept of a tumor immunosurveillance continuum and the molecular continuum between prognostic, predictive, and mechanistic immune signatures (*45*, *46*). It is striking to observe the major impact of the host adaptive immune response on all aspects of the metastatic process, including early metastatic invasion and synchronous and metachronous metastasis.

We conclude that analysis of CRC tumor–related gene expression, cancer driver mutations, and CIN did not reveal tumor factors overexpressed, mutated, amplified, or implicated in metastatic invasion. It appears that each tumor is unique and has a different set of amplifications, deletions, mutations, and personalized tumor-related gene expression profile. This has also been observed previously using aCGH analysis (*27*) or whole-genome sequencing (*47*). In contrast, our comprehensive analysis of the tumor microenvironment revealed the importance of the immune contexture on the metastatic process. The immune effector cells capable of controlling the micrometastatic and

metastatic disease could be the point of convergence resulting from multiple tumor alterations. Is the decrease in adaptive immunity and lymphocyte cytotoxicity within primary tumors a consequence of the presence of synchronous metastases, or rather its cause? Analysis of primary tumors indicates that the cytotoxic/T_H1 immune response is decreasing before the appearance of metastases, as illustrated by analysis of key immune markers in VE^+ and PI^+ patients (Fig. 6). Furthermore, this immune response was also decreased in patients who will develop metachronous metastases, suggesting that immune alterations are an early event in the promotion of the metastatic process. Overall, our data show that distant metastasis is a consequence rather than a cause of the decrease in lymphatic vessels and lymphocyte cytotoxicity seen in CRC tumors, and that the immune phenotype is likely to be a major determinant preventing the synchronous and metachronous spread of tumor cells to distant organs. These results have important clinical implications (*48*) including current clinical trials designed to enhance T lymphocyte function (anti-CTLA4, anti-PD1, and anti-PDL1) and ultimately for successfully treating patients with various cancers (*49*–*52*). Given the success of anti-PD1 immunotherapy in metastatic patients with microsatellite instability (*52*), our data would argue that CRC patients at the early stage may benefit the most from checkpoint T cell therapies, because they have a strong effector T cell response and more frequently present a high Immunoscore. In particular, our study supports the use of T cell–based immunotherapy at early-stage disease to prevent dissemination of tumor cells to develop distant metastases, and also suggests that Immunoscore and the immune analysis of the primary tumor may help predict the presence and development of metastasis.

MATERIALS AND METHODS

Study design

The tumor microenvironment was investigated by different techniques in four randomly selected cohorts of 838 CRC patients. Cohort 1 includes CRC patients from the TCGA project (*22*). Cohorts 2 (n = 205), 3 (n = 109), and 4 (n = 415) include tissue sample material collected at the Laennec–Hôpital Européen Georges Pompidou Hospitals (Paris, France). DNA was available for all patients from cohort 2. Gene expression was tested using Affymetrix microarrays and low-density array (LDA) real-time TaqMan qPCR on samples from cohort 2. TMAs were constructed for 107 samples from cohort 2 and for 415 samples from cohort 3.

A secure Web-based database, TME.db, was built for the management of the patient data from cohorts 2, 3, and 4 (*11*). Ethical, legal, and social implications were approved by ethical review board. Clinical characteristics of the cohorts are described in table S1. The observation time in the cohorts was the interval between diagnosis and last contact (death or last follow-up). Data were censored at the last follow-up for patients without relapse or death. Time to recurrence or disease-free time was defined as the interval from the date of surgery to confirmed tumor relapse date for relapsed patients, and from the date of surgery to the date of last follow-up for disease-free patients.

Publicly available CRC data (TCGA project)

CRC data matrices were downloaded from the TCGA data portal (https://tcga-data.nci.nih.gov/docs/publications/coadread_2012/) on 26 September 2012. Mutation and copy number alteration (GISTIC marker file) data were used. Forty-eight somatic recurrently mutated genes were investigated. Mutations of each gene and of each tested exon were visualized in Genesis. Along the chromosomes, the frequency in the cohort and the mean amplitude of the gain of each gene were used to calculate an amplification score (SCORE = frequency × amplitude). In the same way, a deletion score was calculated. Gene expression profiles generated using RNA-Seq were integrated in the analysis. Additional details on the TCGA data processing were previously described (*22*).

Statistical analysis

The t test and the Wilcoxon-Mann-Whitney test were the parametric and nonparametric tests used to identify markers with a significantly different expression or cell density among patient groups. Fisher's exact test was used to identify overrepresented regions and genes with aberrations. All tests were two-sided. P value less than 0.05 was considered significant. All analyses were performed with the statistical software R implemented as a statistical module in TME.db (*53*). Mutations, genomic alterations, and gene expression levels were visualized using Genesis (*54*).

Cancer-related genes were investigated with Ion Torrent

"Hotspot" regions frequently mutated in 50 human cancer genes were investigated in cohort 2 (n = 214) using the Ion AmpliSeq Cancer Hotspot Panel v2. Forty-eight of these genes that were tested in the TCGA cohort were included in the analysis.

Genomic DNA from 214 patients has been extracted from frozen tumor biopsies using QIAmp DNA Mini kit (Qiagen) or, if frozen samples were not available, from two 5-μm-thick formalin-fixed, paraffin-embedded (FFPE) slides using QIAmp DNA FFPE kit (Qiagen). Quantity of double-strand DNA has been evaluated using qubit 2.0 fluorometer (Invitrogen, Life Technologies), and 10 ng (or 20 ng if FFPE) of extracted DNA was amplified using Ion AmpliSeq Cancer Hotspot Panel v2 (Ion Torrent, Life Technologies) according to the manufacturer's protocol. Briefly, hotspot regions of 50 oncogenes or tumor suppressor genes were amplified using a panel of 207 primer pairs in 17 cycles of PCR (20 cycles for FFPE samples). Amplicons were then digested with FuPa reagent, and samples were separately barcoded with Ion Xpress Barcodes. Ion AmpliSeq Adapters were then added to each sample. DNA banks were then purified using Agencourt AMPure XP Reagent (Beckman Coulter). Purified libraries obtained were amplified using Platinum PCR SuperMix High Fidelity enzyme and purified again with the Agencourt process, following the manufacturer's instructions (Ion AmpliSeq Library kit 2.0, Ion Torrent, Life Technologies). Quality and quantity of each library have been evaluated with High Sensitivity DNA Chip (Agilent Technologies). Patients were then mixed, and libraries obtained were amplified and enriched using the Ion OneTouch 2 system (Ion PGM Template OT2 200, Life Technologies). Sequencing was performed with the Ion Torrent PGM system using Ion 316 or Ion 318 chip and the Ion PGM Sequencing 200 Kit v2 in a 520-cycle run. Runs were aligned using Variant Caller (v4.2.1.0) plug-in compared to Hg19 database, and results were analyzed using Alamut 2.4.1 software (Interactive Biosoftware).

Array comparative genomic hybridization

Samples were homogenized (ceramic beads and FastPrep-24, MP Biomedicals) in 430 μl of a lysis buffer [1 M tris–0.5 M EDTA (pH 8), 20% SDS, proteinase K] and incubated overnight at 37°C. Genomic DNA was extracted by phenol-chloroform extraction and ethanol precipitation. Genomic DNA was resuspended in 200 μl of highly pure water. Concentrations were evaluated by optical density measurement. Samples were labeled using a BioPrime Array CGH Genomic

Labeling Kit according to the manufacturer's instructions (Invitrogen). Test DNA and reference DNA (500 ng) (Promega) were differentially labeled with dCTP-Cy5 and dCTP-Cy3, respectively (GE Healthcare). aCGH was carried out using a whole-genome oligonucleotide microarray platform (Human Genome CGH 44B Microarray Kit, Agilent Technologies). This array consists of ~43,000 60-mer oligonucleotide probes with a spatial resolution of 43 kb. Samples were labeled with the BioPrime Array CGH Genomic Labeling System (Invitrogen) according to the manufacturer's instructions. Further steps were performed according to the manufacturer's protocol (version 6.0). Slides were scanned using a microarray scanner (G2505B), and images were analyzed using CGH Analytics software 3.4.40 (both from Agilent Technologies) with the statistical algorithm ADM-2 (sensitivity threshold was 6.0). Along the chromosomes, the frequency in the cohort and the mean amplitude of the gain of each gene were used to calculate an amplification score (SCORE = frequency × amplitude). In the same way, a deletion score was calculated.

Affymetrix GeneChip analysis

The tissue sample material was snap-frozen within 15 min after surgery and stored in liquid nitrogen. Frozen tumor specimens were randomly selected for RNA extraction. The total RNA was isolated by homogenization with the RNeasy Isolation kit (Qiagen). A bioanalyzer (Agilent Technologies) was used to evaluate the integrity and the quantity of the RNA. From this RNA, 105 Affymetrix gene chips were performed on the HG-U133A Plus platform using the HG-U133A GeneChip 3′ IVT Express Kit. The raw data were normalized using the GCRMA algorithm. Finally, the $\log_2$ intensities of the gene expression data were used for further analysis.

LDA real-time TaqMan qPCR analysis

Tissue sample material was snap-frozen within 15 min after surgery and stored in liquid nitrogen. From this material, frozen tumor specimens were randomly selected for RNA extraction. The total RNA was isolated by homogenization with the RNeasy Isolation kit (Qiagen). A bioanalyzer (Agilent Technologies) was used to evaluate the integrity and the quantity of the RNA. The analyzed RNA samples were all from different patients. Genes representative for the tumor microenvironment were selected for real-time TaqMan analysis. The experiments were all performed according to the manufacturer's instructions (Applied Biosystems). The quantitative real-time TaqMan qPCR analysis was performed using LDAs and the 7900HT Fast Real-Time PCR System (Applied Biosystems). As internal control, 18*S* ribosomal RNA primers and probes were used. The data were analyzed using the SDS software v2.2 (Applied Biosystems) and TME.db statistical module.

TMA immunohistochemistry analysis

TMA from the center (CT) and invasive margin (IM) of colorectal tumors were constructed (*6*). Assessment of the invasive margin area was performed on standard paraffin sections and was based on the histomorphological variance of the tissue. The invasive margin was defined as a region centered on the border separating the host tissue from malignant glands, with an extent of 1 mm. TMA sections were incubated (60 min at room temperature) with monoclonal antibodies against CD3 (SP7), CD4 (Ventana, catalog no. 7904423, clone SP35), CD8 (4B11), CD57 (NK1), T-Bet, CD45RO (OPD4), GZMB (NeoMarkers, catalog no. MS-1799-SO, mouse anti-human IgG2a, clone GrB-7), NKp46 (R&D Systems, catalog no. MAB1850, mouse anti-human IgG2b, clone 195394), CD68 (PGM-1), CD1A (Ab-5), ENG (CD105), PDPN (D2-40), CK (AE1AE3), and CK8 (NeoMarkers). EnVision+ system (enzyme-conjugated polymer backbone coupled to secondary antibodies) and DAB-chromogen were applied (Dako). Double stainings were revealed with phosphate-conjugated secondary antibodies and Fast Blue chromogen. For single stainings, tissue sections were counterstained with Harris hematoxylin. Isotype-matched mouse monoclonal antibodies were used as negative controls. Triple fluorescence stainings were obtained using PerkinElmer Opal kit. Slides were analyzed using an image analysis workstation (Spot Browser, ALPHELYS). Polychromatic high-resolution spot images (740 × 540 pixel, 1.181 μm per pixel resolution) were obtained (magnification, ×200). The density was recorded as the number of positive cells per unit tissue surface area.

Multiplex staining and multispectral imaging

Triple fluorescence stainings were obtained using PerkinElmer Opal kit. The slides were deparaffinized in Clearene and rehydrated in ethanol. Antigen retrieval was performed in Target Antigen Retrieval Solution pH 9.0 (Dako) using microwave incubation (MWT). Primary mouse antibodies for granzyme B (GrzB) (1:100) were incubated for 1 hour in a humidified chamber at room temperature followed by detection using the Anti-Mouse EnVision System HRP Labelled Polymer (Dako). Visualization of GrzB was accomplished using Opal 520 TSA Plus (1:50), after which the slides were placed in Target Antigen Retrieval Solution pH 9.0 and heated using MWT. In a serial fashion, the slides were then incubated with primary mouse antibodies for CD8 (1:100) or NKp46 (1:200) for 1 hour in a humidified chamber at room temperature, followed by detection using the Anti-Mouse EnVision System HRP Labelled Polymer. CD8 and NKp46 were visualized using Opal 670 TSA Plus (1:50). The slides were again placed in Target Antigen Retrieval Solution pH 9.0, subjected to MWT, and then incubated with primary mouse antibodies to CK (1:150) for 1 hour in a humidified chamber at room temperature, followed by detection using the Anti-Mouse EnVision System HRP Labelled Polymer. CK was then visualized using Opal 570 TSA Plus (1:50), and the slides were placed in Target Antigen Retrieval Solution pH 9.0 for MWT. Nuclei were subsequently stained with 4′,6-diamidino-2-phenylindole solution, and the sections were coverslipped using Vectashield HardSet mounting media. With the Opal method, three mouse primary antibodies were sequentially applied to a single slide. The slides were scanned using Mantra System (PerkinElmer), which captured the fluorescent spectra at 20-nm wavelength intervals from 420 to 720 nm with identical exposure times, and combined to create a single stack image. Images of single-stained tissues and unstained tissue were used to extract the spectrum of each fluorophore and of tissue autofluorescence, respectively, and to establish a spectral library required for multispectral unmixing, which was performed by using InForm image analysis software (PerkinElmer).

Cumulative frequency pyramid matrix

Markers were analyzed in pairs in relation to the metastasis status. For each analyzed marker, 2% of the patients with the highest density were taken and then categorized by incrementing by the next 2% of patients with the highest density until it reaches 100% of the patients. Fifty groups were obtained for each marker at the end of this process. The same method was done starting by the 2% of patients, with the lowest density incrementing by the next 2% of patients with the lowest density. The frequency of metastasis was measured for each possible combination of two markers. For each combination, four matrices

were obtained. The first is a combination of groups of patients with the highest density of two markers (High/High), the second is a combination of patients with the highest density for one marker and with the lowest density for the second maker (High/Low), the third is a combination of patients with the lowest density for one marker and with the highest density for the second maker (Low/High), and the last is a combination of groups of patients with the lowest density of two markers (Low/Low) as illustrated in fig. S7. The four matrices were put together to form only one. This allowed us to visualize a continuous process dependent on the density of the markers.

Mouse endoscopy and orthotopic tumor injection model

Mice were anesthetized using isoflurane, and endoscopy was performed. Endoscopic injection of tumor cells was previously described (*14*). For endoscopic injection of tumor cells, a polythene tube (outer diameter, 0.96 mm; inner diameter, 0.58 mm; Smiths Medical International Ltd.) was equipped with a 20-gauge needle (Becton Dickinson). The tube with the needle was inserted into the working channel of the endoscope. Before insertion of the endoscope into the colon of mice, the needle was positioned inside the working channel to avoid damage of the colonic mucosa. After insertion of the endoscope, the needle was pushed out of the working channel under endoscopic control. The tip of the needle was then carefully inserted through the mucosa into the submucosa, and a total volume of 50-μl cell suspension (number of cells as detailed in the respective figure legends) was injected slowly into the submucosa. During subsequent weeks, tumor growth was analyzed at indicated time points using endoscopy.

ClueGO and CluePedia functional analysis

To investigate genes differentially expressed in patient groups defined on the basis of the M stage and/or *FBXW7* mutation, we used ClueGO (*25*), and CluePedia (*26*) Cytoscape (*55*) apps that we have developed. The expression of the genes was compared between M0 and M1 patient groups and in M0 patients with or without *FBXW7* mutation using CluePedia. The biological role of the significantly differentially expressed genes having the highest expression difference in these clinical groups was further investigated in ClueGO. ClueGO presents enriched pathways within a network, interconnected based on the κ score. The size of the nodes shows the term significance after Bonferroni correction. Two visualization styles were used. Pathways were associated in functional groups based on shared genes. Then, the proportion of the genes from the Hi and Lo clusters compared in this analysis was visualized on the same network. Gene Ontology (GO) (*56*), KEGG (*57*), Reactome (*58*), and WikiPathway data (*59*) were used for the analysis. Terms found in the GO interval of 3 to 8, with at least three genes from the initial list representing a minimum of 4%, were selected. Fusion was applied to reduce the redundancy. The Organic algorithm that determines the node positions based on their connectivity was used for organizing the networks.

SUPPLEMENTARY MATERIALS

www.sciencetranslationalmedicine.org/cgi/content/full/8/327/327ra26/DC1

Fig. S1. Mutations of cancer genes in metastatic (M1) and nonmetastatic (M0) CRC patients.
Fig. S2. Genomic alterations in M0 and M1 CRC patients and their functional impact.
Fig. S3. Expression of genes known to be involved in metastasis, tumor progression, and WNT pathway in patients with (M1) or without (M0) metastasis.
Fig. S4. Immune gene expression in tumors from M0 and M1 patients.
Fig. S5. Blood and lymphatic vessels (BV, LV) in patients with (M1) or without (M0) metastasis.
Fig. S6. Intratumoral immune density in M0 and M1 patients.
Fig. S7. The impact of the tumor microenvironment components on metastasis.
Table S1. Clinical characteristic of the cohorts investigated.
Table S2. Forty-eight cancer-related genes tested for mutations shown in Fig. 1A.
Table S3. Association of central mutations in CRC and with clinical parameters.
Table S4. Fifteen cancer-related pathways shown in Fig. 1B.
Table S5. Amplified and deleted genes in M0 and M1 patients from cohorts 1 and 2.
Table S6. Genes involved in metastasis, tumor progression, and WNT pathway.

REFERENCES AND NOTES

1. A. Jemal, R. Siegel, E. Ward, Y. Hao, J. Xu, T. Murray, M. J. Thun, Cancer statistics, 2008. *CA Cancer J. Clin.* **58**, 71–96 (2008).
2. G. C. Prendergast, E. M. Jaffee, Cancer immunologists and cancer biologists: Why we didn't talk then but need to now. *Cancer Res.* **67**, 3500–3504 (2007).
3. I. P. Witz, Tumor–microenvironment interactions: Dangerous liaisons. *Adv. Cancer Res.* **100**, 203–229 (2008).
4. R. R. Langley, I. J. Fidler, Tumor cell-organ microenvironment interactions in the pathogenesis of cancer metastasis. *Endocr. Rev.* **28**, 297–321 (2007).
5. S. Jones, W.-d. Chen, G. Parmigiani, F. Diehl, N. Beerenwinkel, T. Antal, A. Traulsen, M. A. Nowak, C. Siegel, V. E. Velculescu, K. W. Kinzler, B. Vogelstein, J. Willis, S. D. Markowitz, Comparative lesion sequencing provides insights into tumor evolution. *Proc. Natl. Acad. Sci. U.S.A.* **105**, 4283–4288 (2008).
6. J. Galon, A. Costes, F. Sanchez-Cabo, A. Kirilovsky, B. Mlecnik, C. Lagorce-Pagès, M. Tosolini, M. Camus, A. Berger, P. Wind, F. Zinzindohoué, P. Bruneval, P.-H. Cugnenc, Z. Trajanoski, W.-H. Fridman, F. Pagès, Type, density, and location of immune cells within human colorectal tumors predict clinical outcome. *Science* **313**, 1960–1964 (2006).
7. I. Atreya, M. F. Neurath, Immune cells in colorectal cancer: Prognostic relevance and therapeutic strategies. *Expert Rev. Anticancer Ther.* **8**, 561–572 (2008).
8. G. Bindea, B. Mlecnik, W.-H. Fridman, F. Pagès, J. Galon, Natural immunity to cancer in humans. *Curr. Opin. Immunol.* **22**, 215–222 (2010).
9. G. P. Dunn, L. J. Old, R. D. Schreiber, The three Es of cancer immunoediting. *Annu. Rev. Immunol.* **22**, 329–360 (2004).
10. O. J. Finn, Cancer immunology. *N. Engl. J. Med.* **358**, 2704–2715 (2008).
11. B. Mlecnik, M. Tosolini, P. Charoentong, A. Kirilovsky, G. Bindea, A. Berger, M. Camus, M. Gillard, P. Bruneval, W.–H. Fridman, F. Pagès, Z. Trajanoski, J. Galon, Biomolecular network reconstruction identifies T-cell homing factors associated with survival in colorectal cancer. *Gastroenterology* **138**, 1429–1440 (2010).
12. F. Pagès, A. Berger, M. Camus, F. Sanchez-Cabo, A. Costes, R. Molidor, B. Mlecnik, A. Kirilovsky, M. Nilsson, D. Damotte, T. Meatchi, P. Bruneval, P.-H. Cugnenc, Z. Trajanoski, W.-H. Fridman, J. Galon, Effector memory T cells, early metastasis, and survival in colorectal cancer. *N. Engl. J. Med.* **353**, 2654–2666 (2005).
13. E. Wang, M. C. Panelli, V. Monsurró, F. M. Marincola, A global approach to tumor immunology. *Cell. Mol. Immunol.* **1**, 256–265 (2004).
14. G. Bindea, B. Mlecnik, M. Tosolini, A. Kirilovsky, M. Waldner, A. C. Obenauf, H. Angell, T. Fredriksen, L. Lafontaine, A. Berger, P. Bruneval, W. H. Fridman, C. Becker, F. Pagès, M. R. Speicher, Z. Trajanoski, J. Galon, Spatiotemporal dynamics of intratumoral immune cells reveal the immune landscape in human cancer. *Immunity* **39**, 782–795 (2013).
15. J. D. Bui, R. D. Schreiber, Cancer immunosurveillance, immunoediting and inflammation: Independent or interdependent processes? *Curr. Opin. Immunol.* **19**, 203–208 (2007).
16. C. M. Koebel, W. Vermi, J. B. Swann, N. Zerafa, S. J. Rodig, L. J. Old, M. J. Smyth, R. D. Schreiber, Adaptive immunity maintains occult cancer in an equilibrium state. *Nature* **450**, 903–907 (2007).
17. R. D. Schreiber, L. J. Old, M. J. Smyth, Cancer immunoediting: Integrating immunity's roles in cancer suppression and promotion. *Science* **331**, 1565–1570 (2011).
18. I. Romero, F. Garrido, A. M. Garcia-Lora, Metastases in immune-mediated dormancy: A new opportunity for targeting cancer. *Cancer Res.* **74**, 6750–6757 (2014).
19. B. Mlecnik, M. Tosolini, A. Kirilovsky, A. Berger, G. Bindea, T. Meatchi, P. Bruneval, Z. Trajanoski, W.-H. Fridman, F. Pagès, J. Galon, Histopathologic-based prognostic factors of colorectal cancers are associated with the state of the local immune reaction. *J. Clin. Oncol.* **29**, 610–618 (2011).
20. F. Pagès, A. Kirilovsky, B. Mlecnik, M. Asslaber, M. Tosolini, G. Bindea, C. Lagorce, P. Wind, F. Marliot, P. Bruneval, K. Zatloukal, Z. Trajanoski, A. Berger, W.-H. Fridman, J. Galon, In Situ cytotoxic and memory T cells predict outcome in patients with early-stage colorectal cancer. *J. Clin. Oncol.* **27**, 5944–5951 (2009).
21. J. Galon, W.-H. Fridman, F. Pagès, The adaptive immunologic microenvironment in colorectal cancer: A novel perspective. *Cancer Res.* **67**, 1883–1886 (2007).

22. The Cancer Genome Atlas Network, Comprehensive molecular characterization of human colon and rectal cancer. *Nature* **487**, 330–337 (2012).
23. P. Minoo, I. Zlobec, M. Peterson, L. Terracciano, A. Lugli, Characterization of rectal, proximal and distal colon cancers based on clinicopathological, molecular and protein profiles. *Int. J. Oncol.* **37**, 707–718 (2010).
24. L. S. Rozek, C. M. Herron, J. K. Greenson, V. Moreno, G. Capella, G. Rennert, S. B. Gruber, Smoking, gender, and ethnicity predict somatic *BRAF* mutations in colorectal cancer. *Cancer Epidemiol. Biomarkers Prev.* **19**, 838–843 (2010).
25. G. Bindea, B. Mlecnik, H. Hackl, P. Charoentong, M. Tosolini, A. Kirilovsky, W.-H. Fridman, F. Pagès, Z. Trajanoski, J. Galon, ClueGO: A Cytoscape plug-in to decipher functionally grouped gene ontology and pathway annotation networks. *Bioinformatics* **25**, 1091–1093 (2009).
26. G. Bindea, J. Galon, B. Mlecnik, CluePedia Cytoscape plugin: Pathway insights using integrated experimental and in silico data. *Bioinformatics* **29**, 661–663 (2013).
27. D. Tsafrir, M. Bacolod, Z. Selvanayagam, I. Tsafrir, J. Shia, Z. Zeng, H. Liu, C. Krier, R. F. Stengel, F. Barany, W. L. Gerald, P. B. Paty, E. Domany, D. A. Notterman, Relationship of gene expression and chromosomal abnormalities in colorectal cancer. *Cancer Res.* **66**, 2129–2137 (2006).
28. F. Bertucci, S. Salas, S. Eysteries, V. Nasser, P. Finetti, C. Ginestier, E. Charafe-Jauffret, B. Loriod, L. Bachelart, J. Montfort, G. Victorero, F. Viret, V. Ollendorff, V. Fert, M. Giovaninni, J.-R. Delpero, C. Nguyen, P. Viens, G. Monges, D. Birnbaum, R. Houlgatte, Gene expression profiling of colon cancer by DNA microarrays and correlation with histoclinical parameters. *Oncogene* **23**, 1377–1391 (2004).
29. D. X. Nguyen, P. D. Bos, J. Massagué, Metastasis: From dissemination to organ-specific colonization. *Nat. Rev. Cancer* **9**, 274–284 (2009).
30. J. Galon, B. Mlecnik, G. Bindea, H. K. Angell, A. Berger, C. Lagorce, A. Lugli, I. Zlobec, A. Hartmann, C. Bifulco, I. D. Nagtegaal, R. Palmqvist, G. V. Masucci, G. Botti, F. Tatangelo, P. Delrio, M. Maio, L. Laghi, F. Grizzi, M. Asslaber, C. D'Arrigo, F. Vidal-Vanaclocha, E. Zavadova, L. Chouchane, P. S. Ohashi, S. Hafezi-Bakhtiari, B. G. Wouters, M. Roehrl, L. Nguyen, Y. Kawakami, S. Hazama, K. Okuno, S. Ogino, P. Gibbs, P. Waring, N. Sato, T. Torigoe, K. Itoh, P. S. Patel, S. N. Shukla, Y. Wang, S. Kopetz, F. A. Sinicrope, V. Scripcariu, P. A. Ascierto, F. M. Marincola, B. A. Fox, F. Pagès, Towards the introduction of the 'Immunoscore' in the classification of malignant tumours. *J. Pathol.* **232**, 199–209 (2014).
31. P. D. Bos, X. H.-F. Zhang, C. Nadal, W. Shu, R. R. Gomis, D. X. Nguyen, A. J. Minn, M. J. van de Vijver, W. L. Gerald, J. A. Foekens, J. Massagué, Genes that mediate breast cancer metastasis to the brain. *Nature* **459**, 1005–1009 (2009).
32. T. Brabletz, A. Jung, S. Spaderna, F. Hlubek, T. Kirchner, Migrating cancer stem cells—An integrated concept of malignant tumour progression. *Nat. Rev. Cancer* **5**, 744–749 (2005).
33. P. J. Campbell, S. Yachida, L. J. Mudie, P. J. Stephens, E. D. Pleasance, L. A. Stebbings, L. A. Morsberger, C. Latimer, S. McLaren, M.-L. Lin, D. J. McBride, I. Varela, S. A. Nik-Zainal, C. Leroy, M. Jia, A. Menzies, A. P. Butler, J. W. Teague, C. A. Griffin, J. Burton, H. Swerdlow, M. A. Quail, M. R. Stratton, C. Iacobuzio-Donahue, P. A. Futreal, The patterns and dynamics of genomic instability in metastatic pancreatic cancer. *Nature* **467**, 1109–1113 (2010).
34. S. Yachida, S. Jones, I. Bozic, T. Antal, R. Leary, B. Fu, M. Kamiyama, R. H. Hruban, J. R. Eshleman, M. A. Nowak, V. E. Velculescu, K. W. Kinzler, B. Vogelstein, C. A. Iacobuzio-Donahue, Distant metastasis occurs late during the genetic evolution of pancreatic cancer. *Nature* **467**, 1114–1117 (2010).
35. Y.-J. Deng, N. Tang, C. Liu, J.-Y. Zhang, S.-L. An, Y.-L. Peng, L.-L. Ma, G.-Q. Li, Q. Jiang, C.-T. Hu, Y.-N. Wang, Y.-Z. Liang, X.-W. Bian, W.-G. Fang, Y.-Q. Ding, CLIC4, ERp29, and Smac/DIABLO derived from metastatic cancer stem–like cells stratify prognostic risks of colorectal cancer. *Clin. Cancer Res.* **20**, 3809–3817 (2014).
36. C.-C. Chang, H.-H. Lin, J.-K. Lin, C.-C. Lin, Y.-T. Lan, H.-S. Wang, S.-H. Yang, W.-S. Chen, T.-C. Lin, J.-K. Jiang, S.-C. Chang, FBXW7 mutation analysis and its correlation with clinicopathological features and prognosis in colorectal cancer patients. *Int. J. Biol. Markers* **30**, e88–e95 (2015).
37. K. Yumimoto, S. Akiyoshi, H. Ueo, Y. Sagara, I. Onoyama, H. Ueo, S. Ohno, M. Mori, K. Mimori, K. I. Nakayama, F-box protein FBXW7 inhibits cancer metastasis in a non-cell-autonomous manner. *J. Clin. Invest.* **125**, 621–635 (2015).
38. K. Balamurugan, S. Sharan, K. D. Klarmann, Y. Zhang, V. Coppola, G. H. Summers, T. Roger, D. K. Morrison, J. R. Keller, E. Sterneck, FBXW7α attenuates inflammatory signalling by downregulating C/EBPδ and its target gene *Tlr4*. *Nat. Commun.* **4**, 1662 (2013).
39. J. A. Joyce, J. W. Pollard, Microenvironmental regulation of metastasis. *Nat. Rev. Cancer* **9**, 239–252 (2009).
40. S. L. Peng, M. J. Townsend, J. L. Hecht, I. A. White, L. H. Glimcher, T-bet regulates metastasis rate in a murine model of primary prostate cancer. *Cancer Res.* **64**, 452–455 (2004).
41. B. Mlecnik, G. Bindea, H. K. Angell, M. S. Sasso, A. C. Obenauf, T. Fredriksen, L. Lafontaine, A. M. Bilocq, A. Kirilovsky, M. Tosolini, M. Waldner, A. Berger, W. H. Fridman, A. Rafii, V. Valge-Archer, F. Pagès, M. R. Speicher, J. Galon, Functional network pipeline reveals genetic determinants associated with in situ lymphocyte proliferation and survival of cancer patients. *Sci. Transl. Med.* **6**, 228ra37 (2014).
42. G. Bindea, B. Mlecnik, H. K. Angell, J. Galon, The immune landscape of human tumors: Implications for cancer immunotherapy. *Oncoimmunology* **3**, e27456 (2014).
43. T. N. Schumacher, R. D. Schreiber, Neoantigens in cancer immunotherapy. *Science* **348**, 69–74 (2015).
44. M. Angelova, P. Charoentong, H. Hackl, M. L. Fischer, R. Snajder, A. M. Krogsdam, M. J. Waldner, G. Bindea, B. Mlecnik, J. Galon, Z. Trajanoski, Characterization of the immunophenotypes and antigenomes of colorectal cancers reveals distinct tumor escape mechanisms and novel targets for immunotherapy. *Genome Biol.* **16**, 64 (2015).
45. H. Angell, J. Galon, From the immune contexture to the Immunoscore: The role of prognostic and predictive immune markers in cancer. *Curr. Opin. Immunol.* **25**, 261–267 (2013).
46. J. Galon, H. K. Angell, D. Bedognetti, F. M. Marincola, The continuum of cancer immunosurveillance: Prognostic, predictive, and mechanistic signatures. *Immunity* **39**, 11–26 (2013).
47. T. Sjöblom, S. Jones, L. D. Wood, D. W. Parsons, J. Lin, T. D. Barber, D. Mandelker, R. J. Leary, J. Ptak, N. Silliman, S. Szabo, P. Buckhaults, C. Farrell, P. Meeh, S. D. Markowitz, J. Willis, D. Dawson, J. K. V. Willson, A. F. Gazdar, J. Hartigan, L. Wu, C. Liu, G. Parmigiani, B. H. Park, K. E. Bachman, N. Papadopoulos, B. Vogelstein, K. W. Kinzler, V. E. Velculescu, The consensus coding sequences of human breast and colorectal cancers. *Science* **314**, 268–274 (2006).
48. T. J. Hudson, W. Anderson, A. Artez, A. D. Barker, C. Bell, R. R. Bernabé, M. K. Bhan, F. Calvo, I. Eerola, D. S. Gerhard, A. Guttmacher, M. Guyer, F. M. Hemsley, J. L. Jennings, D. Kerr, P. Klatt, P. Kolar, J. Kusada, D. P. Lane, F. Laplace, L. Youyong, G. Nettekoven, B. Ozenberger, J. Peterson, T. S. Rao, J. Remacle, A. J. Schafer, T. Shibata, M. R. Stratton, J. G. Vockley, K. Watanabe, H. Yang, M. M. Yuen, B. M. Knoppers, M. Bobrow, A. Cambon-Thomsen, L. G. Dressler, S. O. Dyke, Y. Joly, K. Kato, K. L. Kennedy, P. Nicolás, M. J. Parker, E. Rial-Sebbag, C. M. Romeo-Casabona, K. M. Shaw,S. Wallace, G. L. Wiesner, N. Zeps, P. Lichter, A. V. Biankin, C. Chabannon, L. Chin, B. Clément, E. de Alava, F. Degos, M. L. Ferguson, P. Geary, D. N. Hayes, A. L. Johns, A. Kasprzyk, H. Nakagawa, R. Penny, M. A. Piris, R. Sarin, A. Scarpa, T. Shibata, M. van de Vijver, P. A. Futreal, H. Aburatani, M. Bayés, D. D. Botwell, P. J. Campbell, X. Estivill, S. M. Grimmond, I. Gut, M. Hirst, C. López-Otín, P. Majumder, M. Marra, J. D. McPherson, H. Nakagawa, Z. Ning, X. S. Puente, Y. Ruan, T. Shibata, M. R. Stratton, H. G. Stunnenberg, H. Swerdlow, V. E. Velculescu, R. K. Wilson, H. H. Xue, L. Yang, P. T. Spellman, G. D. Bader, P. C. Boutros, P. Flicek, G. Getz, R. Guigó, G. Guo, D. Haussler, S. Heath, T. J. Hubbard, T. Jiang, S. M. Jones, Q. Li, N. López-Bigas, R. Luo, L. Muthuswamy, B. F. Ouellette, J. V. Pearson, X. S. Puente, V. Quesada, B. J. Raphael, C. Sander, T. Shibata, T. P. Speed, L. D. Stein, J. M. Stuart, J. W. Teague, Y. Totoki, T. Tsunoda, A. Valencia, D. A. Wheeler, H. Wu, S. Zhao, G. Zhou, L. D. Stein, R. Guigó, T. J. Hubbard, Y. Joly, S. M. Jones, A. Kasprzyk, M. Lathrop, N. López-Bigas, B. F. Oullette, P. T. Spellman, P. T. Spellman, J. W. Teague, G. Thomas, T. Yoshida, K. L. Kennedy, M. Axton, C. Gunter, L. J. Miller, J. Zhang, S. A. Haider, J. Wang, C. K. Yung, A. Cross, Y. Liang, S. Gnaneshan, J. Guberman, J. Hsu, D. R. Chalmers, K. W. Hasel, T. S. Kaan, W. W. Lowrance, T. Masui, L. L. Rodriguez, C. Vergely, D. D. Bowtell, N. Cloonan, A. deFazio, J. R. Eshleman, D. Etemadmoghadam, B. A. Gardiner, J. G. Kench, R. L. Sutherland, M. A. Tempero, N. J. Waddell, P. J. Wilson, S. Gallinger, M. S. Tsao, P. A. Shaw, G. M. Petersen, D. Mukhopadhyay, R. A. DePinho, S. Thayer, K. Shazand, T. Beck, M. Sam, L. Timms, V. Ballin, Y. Lu, J. Ji, X. Zhang, F. Chen, X. Hu, Q. Yang, G. Tian, L. Zhang, X. Xing, X. Li, Z. Zhu, Y. Yu, J. Yu, J. Tost, P. Brennan, I. Holcatova, D. Zaridze, A. Brazma, L. Egevard, E. Prokhortchouk, R. E. Banks, M. Uhlen, J. Viksna, F. Ponten, K. Skryabin, E. Birney, A. Borg, A. L. Borresen-Dale, C. Caldas, J. A. Foekens, S. Martin, J. S. Reis-Filho, A. L. Richardson, C. Sotiriou, G. Thoms, L. van't Veer, D. Birnbaum, H. Blanche, P. Boucher, S. Boyault, J. D. Masson-Jacquemier, I. Pauporte, X. Pivot, A. Vincent-Salomon, E. Tabone, C. Theillet, I. Treilleux, P. Bioulac-Sage, T. Decaens, D. Franco, M. Gut, D. Samuel, J. Zucman-Rossi, R. Eils, B. Brors, J. O. Korbel, A. Korshunov, P. Landgraf, H. Lehrach, S. Pfister, B. Radlwimmer, G. Reifenberger, M. D. Taylor, C. von Kalle, P. P. Majumder, P. Pederzoli, R. A. Lawlor, M. Delledonne, A. Bardelli, T. Gress, D. Klimstra, G. Zamboni, Y. Nakamura, S. Miyano, A. Fujimoto, E. Campo, S. de Sanjose, E. Montserrat, M. Gonzalez-Diaz, P. Jares, H. Himmelbaue, S. Bea, S. Aparicio, D. F. Easton, F. S. Collins, C. C. Compton, E. S. Lander, W. Burke, A. R. Green, S. R. Hamilton, O. P. Kallioniemi, T. J. Ley, E. T. Liu, B. J. Wainwright, International network of cancer genome projects. *Nature* **464**, 993–998 (2010).
49. D. M. Pardoll, The blockade of immune checkpoints in cancer immunotherapy. *Nat. Rev. Cancer* **12**, 252–264 (2012).
50. M. Vanneman, G. Dranoff, Combining immunotherapy and targeted therapies in cancer treatment. *Nat. Rev. Cancer* **12**, 237–251 (2012).
51. F. S. Hodi, S. J. O'Day, D. F. McDermott, R. W. Weber, J. A. Sosman, J. B. Haanen, R. Gonzalez, C. Robert, D. Schadendorf, J. C. Hassel, W. Akerley, A. J. M. van den Eertwegh, J. Lutzky, P. Lorigan, J. M. Vaubel, G. P. Linette, D. Hogg, C. H. Ottensmeier, C. Lebbé, C. Peschel, I. Quirt, J. I. Clark, J. D. Wolchok, J. S. Weber, J. Tian, M. J. Yellin, G. M. Nichol, A. Hoos, W. J. Urba, Improved survival with ipilimumab in patients with metastatic melanoma. *N. Engl. J. Med.* **363**, 711–723 (2010).
52. D. T. Le, J. N. Uram, H. Wang, B. R. Bartlett, H. Kemberling, A. D. Eyring, A. D. Skora, B. S. Luber, N. S. Azad, D. Laheru, B. Biedrzycki, R. C. Donehower, A. Zaheer, G. A. Fisher, T. S. Crocenzi, J. J. Lee, S. M. Duffy, R. M. Goldberg, A. de la Chapelle, M. Koshiji, F. Bhaijee, T. Huebner, R. H. Hruban, L. D. Wood, N. Cuka, D. M. Pardoll, N. Papadopoulos, K. W. Kinzler, S. Zhou, T. C. Cornish, J. M. Taube, R. A. Anders, J. R. Eshleman, B. Vogelstein, L. A. Diaz Jr., PD-1 blockade in tumors with mismatch-repair deficiency. *N. Engl. J. Med.* **372**, 2509–2520 (2015).
53. B. Mlecnik, F. Sanchez-Cabo, P. Charoentong, G. Bindea, F. Pagès, A. Berger, J. Galon, Z. Trajanoski, Data integration and exploration for the identification of molecular mechanisms in tumor-immune cells interaction. *BMC Genomics* **11** (Suppl. 1), S7 (2010).

54. A. Sturn, J. Quackenbush, Z. Trajanoski, Genesis: Cluster analysis of microarray data. *Bioinformatics* **18**, 207–208 (2002).
55. P. Shannon, A. Markiel, O. Ozier, N. S. Baliga, J. T. Wang, D. Ramage, N. Amin, B. Schwikowski, T. Ideker, Cytoscape: A software environment for integrated models of biomolecular interaction networks. *Genome Res.* **13**, 2498–2504 (2003).
56. M. Ashburner, C. A. Ball, J. A. Blake, D. Botstein, H. Butler, J. M. Cherry, A. P. Davis, K. Dolinski, S. S. Dwight, J. T. Eppig, M. A. Harris, D. P. Hill, L. Issel-Tarver, A. Kasarskis, S. Lewis, J. C. Matese, J. E. Richardson, M. Ringwald, G. M. Rubin, G. Sherlock, Gene ontology: Tool for the unification of biology. The Gene Ontology Consortium. *Nat. Genet.* **25**, 25–29 (2000).
57. M. Kanehisa, S. Goto, S. Kawashima, A. Nakaya, The KEGG databases at GenomeNet. *Nucleic Acids Res.* **30**, 42–46 (2002).
58. D. Croft, G. O'Kelly, G. Wu, R. Haw, M. Gillespie, L. Matthews, M. Caudy, P. Garapati, G. Gopinath, B. Jassal, S. Jupe, I. Kalatskaya, S. Mahajan, B. May, N. Ndegwa, E. Schmidt, V. Shamovsky, C. Yung, E. Birney, H. Hermjakob, P. D'Eustachio, L. Stein, Reactome: A database of reactions, pathways and biological processes. *Nucleic Acids Res.* **39**, D691–D697 (2011).
59. T. Kelder, M. P. van Iersel, K. Hanspers, M. Kutmon, B. R. Conklin, C. T. Evelo, A. R. Pico, WikiPathways: Building research communities on biological pathways. *Nucleic Acids Res.* **40**, D1301–D1307 (2012).

Funding: This work was supported by grants from the National Cancer Institute of France (INCa), Canceropole Ile de France, Ville de Paris, MedImmune, INSERM, European Commission (7FP, Geninca Consortium, grant 202230), Cancer Research for Personalized Medicine (CARPEM), European Commission (H2020, PHC32, APERIM), Paris Alliance of Cancer Research Institutes (PACRI), and LabEx Immuno-oncology. **Author contributions:** A.K., M.T., T.F., S.M., A.V., and M.W. acquired the tumor microenvironment data. A.C.O., T.F., and M.R.S. acquired the genomic data. B.M., G.B., and A.K. analyzed the data. A.B. was responsible for clinical data. B.M., G.B., A.K., and J.G. interpreted the data. J.G. designed and supervised the study. B.M., G.B., A.K., and J.G. wrote the manuscript. S.E.C., P.M., M.A., F.P., M.R.S., H.K.A., and V.V.-A. revised the manuscript. **Competing interests:** B.M., G.B., F.P., and J.G. have patents on methods and kits for screening patients with cancer. J.G. is a co-founder of HalioDx Company.

Submitted 14 October 2015
Accepted 28 January 2016
Published 24 February 2016
10.1126/scitranslmed.aad6352

Citation: B. Mlecnik, G. Bindea, A. Kirilovsky, H. K. Angell, A. C. Obenauf, M. Tosolini, S. E. Church, P. Maby, A. Vasaturo, M. Angelova, T. Fredriksen, S. Mauger, M. Waldner, A. Berger, M. R. Speicher, F. Pagès, V. Valge-Archer, J. Galon, The tumor microenvironment and Immunoscore are critical determinants of dissemination to distant metastasis. *Sci. Transl. Med.* **8**, 327ra26 (2016).

Science Translational Medicine
AAAS

The tumor microenvironment and Immunoscore are critical determinants of dissemination to distant metastasis

Bernhard Mlecnik, Gabriela Bindea, Amos Kirilovsky, Helen K. Angell, Anna C. Obenauf, Marie Tosolini, Sarah E. Church, Pauline Maby, Angela Vasaturo, Mihaela Angelova, Tessa Fredriksen, Stéphanie Mauger, Maximilian Waldner, Anne Berger, Michael R. Speicher, Franck Pagès, Viia Valge-Archer and Jérôme Galon

(February 24, 2016)
Science Translational Medicine **8** (327), 327ra26. [doi: 10.1126/scitranslmed.aad6352]

Editor's Summary

Managing metastasis

Because of the poor prognosis of metastatic cancer, it is critical to determine exactly how different factors contribute to cancer spread. Mlecnik *et al*. examined the impact of tumor-intrinsic, microenvironmental, and immunological factors on tumor metastasis in colorectal cancer patients. They found that decreased presence of lymphatic vessels and reduced immune cytotoxicity were more strongly associated with the metastatic process than tumor-intrinsic factors such as chromosomal instability or cancer-associated mutations. These data support testing the Immunoscore as a biomarker to predict metastasis and guide therapy.

Science Translational Medicine (print ISSN 1946-6234; online ISSN 1946-6242) is published weekly, except the last week in December, by the American Association for the Advancement of Science, 1200 New York Avenue, NW, Washington, DC 20005.

Science Translational Medicine (print ISSN 1946-6234; online ISSN 1946-6242) is published weekly, except the last week in December, by the American Association for the Advancement of Science, 1200 New York Avenue, NW, Washington, DC 20005.